Impact of HO$_2$/RO$_2$ ratio on highly oxygenated α-pinene photooxidation products and secondary organic aerosol formation potential

Yarê Baker[1], Sungah Kang[1], Hui Wang[1], Rongrong Wu[1], Jian Xu[1], Annika Zanders[1], Quanfu He[1], Thorsten Hohaus[1], Till Ziehm[1], Veronica Geretti[2], Thomas J. Bannan[3], Simon P. O'Meara[3,4], Aristeidis Voliotis[3], Mattias Hallquist[2], Gordon McFiggans[3], Sören R. Zorn[1], Andreas Wahner[1], and Thomas F. Mentel[1]

[1]Institute for Energy and Climate Research, IEK-8, Forschungszentrum Jülich, 52425 Jülich, Germany
[2]Atmospheric Science, Dept. of Chemistry, University of Gothenburg, Gothenburg, 412 96, Sweden
[3]Department for Earth and Environmental Sciences, University of Manchester, Manchester, M13 9PL, UK
[4]National Centre for Atmospheric Science, University of Manchester, Manchester, M13 9PL, UK

Correspondence to: Thomas F. Mentel (t.mentel@fz-juelich.de)

Abstract. Highly oxygenated molecules (HOMs) from the atmospheric oxidation of biogenic volatile organic compounds are important contributors to secondary organic aerosol (SOA). Organic peroxy radicals (RO$_2$) and hydroperoxy radicals (HO$_2$) are key species influencing the HOM product distribution. In laboratory studies experimental requirements often result in overemphasis of RO$_2$ cross-reactions compared to reactions of RO$_2$ with HO$_2$. We analyzed the photochemical formation of HOMs from α-pinene and their potential to contribute to SOA formation under high (≈1/1) and low (≈1/100) HO$_2$/RO$_2$ conditions. As HO$_2$/RO$_2$ > 1 is prevalent in the daytime atmosphere, sufficiently high HO$_2$/RO$_2$ is crucial to mimic atmospheric conditions and to prevent biases by low HO$_2$/RO$_2$ on the HOM product distribution and thus SOA yield. Experiments were performed under steady-state conditions in the new, continuously stirred tank reactor SAPHIR-STAR at Forschungszentrum Jülich. The HO$_2$/RO$_2$ ratio was increased by adding CO, while keeping the OH concentration constant. We determined the HOM's SOA formation potential, considering their fraction remaining in the gas phase after seeding with (NH$_4$)$_2$SO$_4$ aerosol. Increase of HO$_2$/RO$_2$ led to a reduction in SOA formation potential, with the main driver being a ≈60% reduction in HOM-accretion products. We also observed a shift in HOM-monomer functionalization from carbonyl to hydroperoxide groups. We determined a reduction of the HOM's SOA formation potential by ≈30 % at HO$_2$/RO$_2$≈1/1 compared to HO$_2$/RO$_2$≈1/100. Particle phase observations measured an about according decrease in SOA mass and yield. Our study showed that too low HO$_2$/RO$_2$ ratios compared to the atmosphere can lead to an overestimation of SOA yields.

1   Introduction

In the atmosphere highly oxidized products from the oxidation of biogenic or anthropogenic volatile organic compounds (VOCs) are an important source of secondary organic aerosol (SOA) (Roldin et al., 2019; Mohr et al., 2019). SOA is an important contributor to the overall ambient aerosol and of interest because of its impact on climate, visibility, and human health (Hallquist et al., 2009).

Recently, many studies (Pullinen et al., 2020; Berndt et al., 2016; Bianchi et al., 2017) have focused on understanding the oxidation pathways of VOCs that yield highly oxygenated molecules (HOMs), as these are expected to be of low enough volatility to condense into the particle phase. One important tool for the investigation of VOC degradation and SOA formation is the utilization of experiments in atmospheric simulation chambers (Hidy, 2019). Such experiments have also helped to elucidate key processes in the HOM formation, i.e. the process of autoxidation.

After an initial oxidant attack and the formation of a peroxy radical (RO_2), autoxidation adds oxygen to the molecule via an internal H-shift to the peroxy group, forming a hydroxy peroxide group and an alkyl radical, to which O_2 immediately adds, reestablishing the peroxy functionality. This process can be repeated multiple times yielding almost instantaneously highly oxygenated peroxy radicals (HOM-RO_2) which are terminated to a series of HOM closed-shell products (Bianchi et al., 2019; Ehn et al., 2014; Crounse et al., 2013).

Chamber studies often work with a singular compound and operate at higher precursor concentrations than those observed in the atmosphere for experimental reasons. These experiments cannot represent the complex mixture of VOCs and oxidized VOCs present in the atmosphere (McFiggans et al., 2019). Higher precursor concentrations can lead per se to higher SOA yields than observed in the atmosphere (a well characterized phenomenon (see Henry et al. (2012), Shilling et al. (2009)) and to a general preference of higher order processes which may not be important in the atmosphere. One example is that chamber studies tend to overestimate the role of cross reactions between organic peroxy radicals (RO_2) owing to high precursor concentrations of a single VOC. In chambers, reactions of HOM-RO_2 with other organic peroxy radicals terminate the autoxidation chain, leading typically to multifunctional carbonyl and alcohol compounds. In comparison, in the atmosphere termination by HO_2 is more likely, leading to multifunctional hydroperoxides. In presence of sufficient NO, termination to multifunctional organic nitrates may be more important (Schervish and Donahue, 2021).

Another possible termination reaction of HOM-RO_2 with HOM-RO_2 and less oxidized RO_2 leads to the formation of accretion products, which are expected to be extremely low volatile organic compounds (ELVOCs) and are therefore expected to contribute to new particle formation and SOA formation (Ehn et al., 2014; Berndt et al., 2018). Schervish and Donahue (2021) raised awareness that chamber studies could overestimate the SOA formation potential from the oxidation of terpenes such as α-pinene compared to the atmosphere, because of missing HO_2 and small RO_2 (e.g. CH_3O_2), which favors accretion product formation. Previous studies of VOC ozonolysis with different OH scavengers by Docherty and Ziemann (2003) and Keywood et al. (2004), indicated a significant impact of the HO_2/RO_2 ratio on SOA yields.

61 In chamber studies the use of higher VOC concentrations is often an unavoidable necessity either to match the sensitivity of

62 the analytical instrumentation or to overcome chamber related effects. The question remains, how can conditions dictated by

63 the chamber be steered towards more realistic chemical pathways and higher atmospheric relevance?

64 In this study we address this overestimated importance of peroxy radical cross reactions. We studied the photooxidation of α-

65 pinene in a series of steady-state experiments in the newly built continuously stirred tank reactor SAPHIR-STAR (a

66 modernized version of JPAC, see Mentel et al. (2009)).

67 We compared two experimental conditions, a pure α-pinene photooxidation case leading to low HO_2/RO_2 ratios and high

68 importance of RO_2 cross-reactions and a high HO_2/RO_2 case representing more atmospheric relevant conditions with high

69 importance of $RO_2 + HO_2$ reactions. One important concept of the conducted experiments is the constant OH availability to

70 α-pinene in order to prevent effects of different oxidant levels and allow for a direct comparison between the two chemical

71 regimes. To this end, the OH concentration in the experiments was adjusted to keep the α-pinene OH turnover constant and

72 to avoid changes due to oxidant scavenging.

73 Furthermore, the addition of seed particles ($(NH_4)_2SO_4$) allowed us to observe the condensation behavior of the HOM-

74 products and to compare our gas phase observations directly with particulate phase measurements of the condensed organic

75 mass.

76 In this study we will address two central questions: How does the shift in HO_2/RO_2 impact the oxidation mechanism of

77 α-pinene, especially the HOM formation pathway? And what is the subsequent impact on the SOA formation potential of the

78 α-pinene photooxidation system? As the central analysis tool, we will use high resolution time of flight mass spectrometry

79 with chemical ionization (HR-TOF-CIMS) with nitrate (NO_3^-) reagent ions as this ionization scheme is selective towards

80 HOM compounds (Hyttinen et al., 2018).

81 ## 2   Methods

82 ### 2.1   Generic α-pinene HOM peroxy radical chemistry

83 The chemical mechanistic information for the basic oxidation scheme of α-pinene was taken from the Master Chemical

84 Mechanism MCM v3.3.1 (Jenkin et al., 1997; Saunders et al., 2003) (http://mcm.york.ac.uk). The main peroxy radicals

85 expected from α-pinene photooxidation are $C_{10}H_{17}O_x$ and $C_{10}H_{15}O_x$. $C_{10}H_{17}O_x$ is formed by the addition of OH to α-pinene,

86 followed by O_2 (starting RO_2: $C_{10}H_{17}O_3$) (MCM v3.3.1 (Jenkin et al., 1997; Saunders et al., 2003)). Studies showed that the

87 autoxidation can start from $C_{10}H_{17}O_3$ with the four-member ring in α-pinene opened (Berndt, 2021; Xu et al., 2019).

88 For $C_{10}H_{15}O_x$ the autoxidation chain is assumed to start with $C_{10}H_{15}O_4$, which can be formed directly from ozonolysis via the

89 vinyl hydroperoxide path (Johnson and Marston, 2008; Iyer et al., 2021) or via H-abstraction from first-generation oxidation

90 products such as pinonaldehyde ($C_{10}H_{16}O_2$). (MCM v3.3.1 (Jenkin et al., 1997; Saunders et al., 2003; Fantechi et al., 2002).

91 A recent study suggests direct H-abstraction by OH from α-pinene (Shen et al., 2022) as a starting point for the autoxidation
92 chain.

93 The autoxidation process is rapid with H-shift rates of about 0.01 - 0.1 s^{-1} and faster (Piletic and Kleindienst, 2022; Berndt,
94 2021; Xu et al., 2019; Vereecken et al., 2007). The autoxidation chain will run quickly, adding more oxygen to the molecule,
95 until bimolecular termination reactions are able to compete with all available H-shift rates. The rate of an H-shift is
96 determined by the hydrogen's position in relation to the peroxy radical and the functional groups near the hydrogen and
97 peroxy radical (Otkjaer et al., 2018; Vereecken and Nozière, 2020). In the absence of NO_x, the peroxy radicals have two
98 major bimolecular termination channels: the reaction with another RO_2 or with HO_2. A third pathway is the intramolecular
99 termination (Rissanen et al., 2014).

100 Based on the considerations above, we apply a simplified generic reaction scheme to analyze our observations. **Figure 1**
101 shows an overview of the reaction pathways for the main peroxy radical families in the α-pinene photooxidation and the
102 resulting product groups and families. The compounds can be separated into four classes; peroxy radicals (HOM-RO_2),
103 monomers (HOM-Mon), accretion products (HOM-Acc) and fragments (HOM-Frag). The HOM-RO_2 class consists of all
104 detected HOM-RO_2, with special focus on the analysis of the C_{10} HOM-RO_2 family. The HOM-Mon class contains the
105 closed-shell HOM-C_{10} products. The compounds in the fragment class contain less than ten carbon atoms, while all
106 HOM-Acc compounds contain more than ten carbon atoms. The compound classes are further divided into groups and
107 families. Here, the term group is used for compounds with the same carbon number, while a family contains all compounds
108 with the same carbon and hydrogen number but a varying oxygen number.
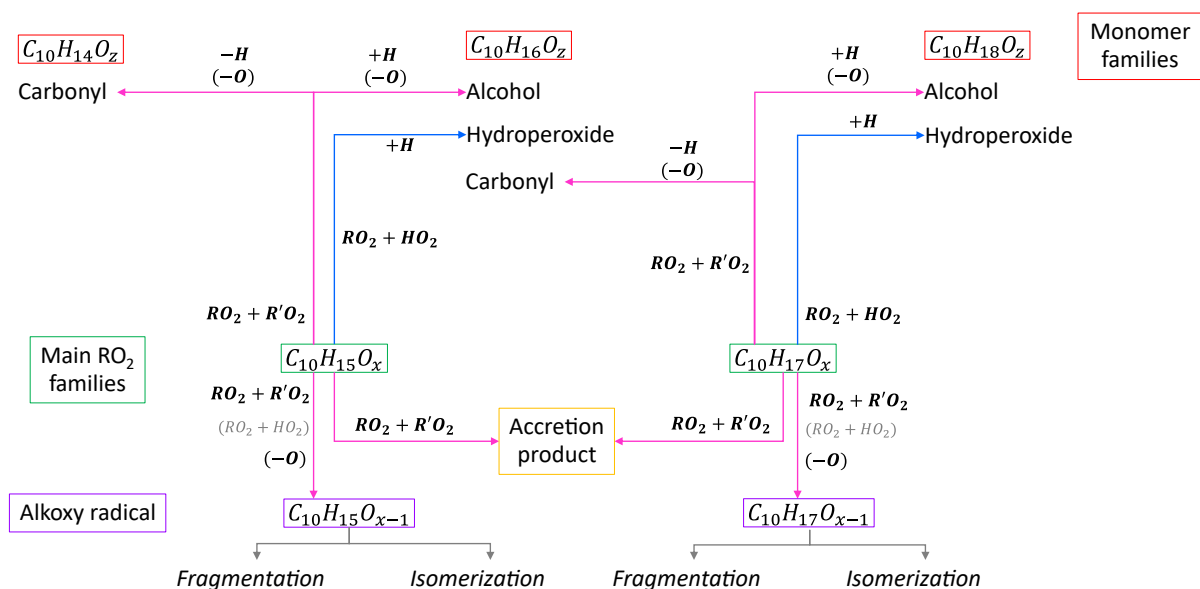
109
110 **Figure 1: Overview of important reaction pathways of α-pinene RO_2 with other RO_2 and HO_2.**

111   The termination of RO_2 with HO_2 will lead to hydroperoxide formation:

$$RO_2 + HO_2 \rightarrow ROOH + O_2 \qquad\qquad\qquad (R1)$$

112   In the case of $C_{10}H_{15}O_x$, reaction (R1) will lead to multifunctional $C_{10}H_{16}O_z$ hydroperoxides (wherein the notation
113   "hydroperoxides" or "carbonyls", "alcohols" etc. here and in the following relates to the functionality of the group formed by
114   the termination reaction). For $C_{10}H_{17}O_x$ it will lead to the formation of $C_{10}H_{18}O_z$ hydroperoxides. The termination via
115    $RO_2 + RO_2$ can either result in the formation of accretion products or in the formation of carbonyls and alcohols. For the
116   accretion product formation, it is assumed that the two RO_2 chemically bond eliminating O_2 from the molecule:

$$RO_2 + R'O_2 \rightarrow R\text{-}O\text{-}O\text{-}R' + O_2 \qquad\qquad\qquad (R2)$$

117   Recombination reactions of the main peroxy radical families $C_{10}H_{15}O_x$ and $C_{10}H_{17}O_x$ lead to the product families $C_{20}H_{30}O_z$
118   (combination of two $C_{10}H_{15}O_x$), $C_{20}H_{32}O_z$ (combination of $C_{10}H_{15}O_x$ and $C_{10}H_{17}O_x$), and $C_{20}H_{34}O_z$ (combination of two
119    $C_{10}H_{17}O_x$).

120   However, due to reactions with smaller peroxy radicals, HOM-Acc families with smaller carbon and hydrogen numbers are
121   also observed. Indeed, one reason why the $RO_2 + R'O_2$ termination is expected to affect the SOA formation potential is the
122   formation of accretion products by scavenging of less oxidized and smaller RO_2 by HOM-RO_2. Thus, the smaller RO_2 will
123   also contribute to the SOA mass which would otherwise not be the case. For the HOM-RO_2 itself, it is expected that they
124   contribute to SOA formation independently of the termination pathway, due to the low volatility of its expected termination
125   products (Pullinen et al., 2020; McFiggans et al., 2019).

126   The second $RO_2 + R'O_2$ termination pathway is the formation of a carbonyl and alcohol compound:

$$RO_2 + R'O_2 \rightarrow R\text{-}OH + R'\text{=}O + O_2 \qquad\qquad\qquad (R3)$$

127   In this reaction both radicals lose an oxygen atom, and a hydrogen atom is transferred to the RO_2 forming the alcohol
128   termination group. Preferences of RO_2 to form an alcohol or carbonyl compound are possible for individual reactions, but
129   statistically carbonyl and alcohols should be formed with the same fractions. Since mass spectrometry can only determine
130   formula composition, we cannot distinguish alcohols and hydroperoxides, which arise from RO_2 differing by one O atom.
131   Therefore, details of balance of alcohol and carbonyl formation cannot be detected.

132   However, the formula composition can help to differentiate certain formation pathways. The $C_{10}H_{14}O_z$ family contains only
133   carbonyl formed from a $C_{10}H_{15}O_x$ RO_2 while the alcohol will be part of the $C_{10}H_{16}O_z$ family. The $C_{10}H_{16}O_z$ family also
134   contains the carbonyl produced from the $RO_2 + R'O_2$ monomer termination of $C_{10}H_{17}O_x$, while the alcohol from this RO_2
135   family will be found in the $C_{10}H_{18}O_z$ family. So, from a diagnostic point of view, $C_{10}H_{14}O_z$ as well as $C_{10}H_{18}O_z$ are uniquely
136   related to a precursor radical family.

137 The classification of the formation pathways of the monomers is helpful to analyze the effect of the HO_2/RO_2 ratio shift in

138 the experiments. Considering the termination pathways, a decrease in the $C_{10}H_{14}O_z$ family and an increase of the $C_{10}H_{18}O_z$

139 family is expected with increasing HO_2/RO_2 because of increasing termination by HO_2 and decreasing termination by RO_2.

140 In case of $C_{10}H_{18}O_z$ the increase of hydroperoxides is partially compensated by a decrease of the alcohol channel. For

141 $C_{10}H_{16}O_z$ the situation is more complicated as it contains contributions from all termination pathways.

142 Besides closed-shell products, HOM-RO_2 can also form alkoxy radicals (HOM-RO). In general, alkoxy radicals (RO) are

143 important intermediates in the oxidation scheme of organics and are formed via *(R4)* and probably also via *(R5)* for specific

144 RO_2 (Jenkin et al., 2019):

$$RO_2 + R'O_2 \rightarrow RO + R'O + O_2 \tag{R4}$$

$$RO_2 + HO_2 \rightarrow RO + OH + O_2 \tag{R5}$$

145 In reaction *(R5)* OH will be formed. The importance of reaction *(R5)* compared to reaction *(R1)* is still unclear in the

146 literature, but functionalization of the RO_2 close to the peroxy functionality possibly enables this reaction (Iyer et al., 2018;

147 Eddingsaas et al., 2012; Hasson et al., 2005; Jenkin et al., 2019). If reaction *(R5)* is of negligible importance, the reaction

148 scheme will simplify and the effect of increased HO_2/RO_2 is easier to diagnose.

149 We are interested in the importance of alkoxy radical formation as (HOM)-RO tend to fragment, leading to the formation of

150 smaller products (Vereecken et al., 2007). In the context of SOA formation, these fragments are less likely to contribute to

151 SOA mass because of their higher volatility. Since alkoxy radicals are too unstable to be detected directly we use two

152 diagnosis tools to judge the importance of HOM-RO. Firstly, HOM-RO fragmentation can lead to HOM-RO_2 with less than

153 10 carbon atoms which may also continue the autoxidation chain. Therefore, the abundance of HOM with less than 10

154 carbon atoms (HOM-Frag) indicates the importance of alkoxy steps. Secondly, with increasing functionalization, H-shifts

155 retaining the carbon backbone become more likely (Vereecken et al., 2007) which will lead to a next generation of C_{10}-

156 HOM-RO_2. Such alkoxy peroxy steps can continue the autoxidation chain (Mentel et al., 2015). Interestingly, by coupling of

157 an alkoxy and a peroxy step, the parity of the number of oxygen atoms in the HOM-RO_2 changes, while in pure autoxidation

158 steps the oxygen parity remains the same. Therefore, a parity change of the oxygen number can be used as an indication of

159 alkoxy step abundance (Kang, 2021).

160 In summary we will use the changes in contribution and relative signal of the different families and classes to judge the

161 impact of shifting from low to high HO_2/RO_2 on the α-pinene photooxidation pathway.

162 **2.2   Control of α-pinene OH turnover**

163 After the initial α-pinene photooxidation phase as a reference, CO was added to the oxidation system. The idea is to

164 represent small, oxidized VOCs in the atmosphere that can produce HO_2 by reaction with OH (compare Schervish and

165 Donahue (2021)). Presence of CO shifts the HO_2 to RO_2 ratio, increasing the importance of the termination of RO_2 by HO_2.

166 McFiggans et al. (2019) showed that one limiting factor in mixture experiments is oxidant scavenging: the products and their

167 yields in mixed systems change, because there is less OH available to the individual VOC. Thus, after the CO addition the

168 OH production in the chamber was increased to compensate for the OH consumed by CO. The OH levels in the system

169 before and after the CO addition were approximately the same, keeping the α-pinene OH turnover approximately constant.

170 This OH adjustment ensures that the primary α-pinene chemistry was kept the same, avoiding effects by different oxidant

171 levels, and enabling a direct comparison.

172 However, since experiments could only be performed at *about* the same OH levels, a normalization by the actual α-pinene

173 OH turnover is applied to the data. This compensates for the slight experimental imperfections and enables better

174 comparison of experiment series with different boundary conditions. The turnover in steady state is given in **Eq. (1)**. Here

175 the subscript "SS" denotes steady state condition for the concentrations of α-pinene and OH, k_{OH} is the α-pinene OH reaction

176 rate constant.

$$turnover_{apinene+OH} = k_{OH} * [α\text{-}pinene]_{SS} * [OH]_{SS} \tag{1}$$

177 This normalization also directly shows the yield of certain oxidation product or product group per α-pinene consumed by

178 OH.

2.3 Derivation of effect on condensable mass from gas-phase measurement

180 A simple proxy for the condensable mass from HOM products can be calculated from the steady-state HOM-signals

181 measured by the NO_3-CIMS, assuming condensation for all low volatility HOM-compounds and no back evaporation into

182 the gas phase. To only take low volatility products into account we used all detected formula compositions with

183 M> 230 g mol^{-1} and weighted them with their molar mass. The reasoning behind this threshold can be found in **Sect. 4.4**. All

184 contributions were summed up and normalized with the α-pinene OH turnover for the comparison between the low and high

185 HO_2/RO_2 cases (**Eq. (2)**).

$$mass\ weighted\ signal\ sum = \frac{\sum_{i=0}^{i} S_i * M_i}{turnover_{apinene+OH}} \tag{2}$$

186 We also estimated the expected SOA mass formed using the calibration factor obtained for sulfuric acid for our NO_3-CIMS

187 instrument in a calibration setup (see supplement **Sect. S1**). From this we calculated an upper boundary concentration of

188 detected HOM-compounds in the gas phase under the assumption that sulfuric acid clusters with nitrate at the collision limit,

189 yielding maximum sensitivity (a common approach, see for example Ehn et al. (2014), Pullinen et al. (2020)).

190 The calculated gas phase concentration was then used in the steady state equation describing the relationship between gas

191 and particle phase concentrations of a single compound *i* shown in **Eq. (3)**.

$$m_{i,seed}(p) = \frac{m_{i,seed}(g) * k_{cond,i}}{k_{particleLoss} + k_{evap,i}} \tag{3}$$

192 **Equation (3)** shows that the steady state particle phase (mass) concentration $m_{i,seed}(p)$ of compound i in presence of seed in

193 the chamber is only dependent on the steady state gas phase concentration $m_{i,seed}(g)$, the condensation rate and evaporation

194 rate constants $k_{cond,i}$, $k_{evap,i}$ of i (to and from the particles) and the particle loss rate constant $k_{particleLoss}$ in the chamber.

195 The condensation rate can be calculated (see supplement **Sect. S8**), and the particle loss rate constant was measured by

196 observation of the particle loss in the chamber after ending the seed addition (details in the supplement **Sect. S2**). The

197 evaporation rate was assumed to be negligible for the investigated HOM-compounds.

198 For the SOA yield calculation, we calculate a corrected organic mass m_{SOA} from the organic mass m_{AMS} measured by aerosol

199 mass spectrometry (AMS) and the fraction expected to be lost on the seed particles compared to the overall loss on particles

200 and chamber wall as shown in **Eq. (4)** (McFiggans et al., 2019).

$$m_{SOA} = m_{AMS} * \frac{k_{cond} + k_{wall}}{k_{cond}} \tag{4}$$

201 In **Eq. (4)** we use the condensation rate constant k_{cond} calculated for one major HOM-product ($C_{10}H_{16}O_7$) and the average

202 HOM-Mon wall loss rate k_{wall} which was determined by switching off the UVC light and observing the decay of

203 photooxidation products in the NO₃-CIMS. The wall loss determination, as well as SOA mass correction were described

204 before in Sarrafzadeh et al. (2016) and McFiggans et al. (2019).

205 **3   Experimental methods**

206 **3.1   Chamber setup**

207 Experiments were conducted in the Jülich SAPHIR STAR chamber, which is the modern successor of the JPAC setup

208 (Mentel et al., 2009). The basic concepts are the same as in JPAC, but each parameter is set, controlled, and monitored in a

209 program. The chamber was operated as a continuously stirred tank reactor. It is a borosilicate glass cylinder (l=2.5 m, d=1 m)

210 with a volume of close to 2000 L and all equipment inside the chamber is either glass or glass coated steel (SilcoTek

211 GmbH).

212 With an inflow of 32 L min⁻¹, the residence time in the chamber was approximately 61 minutes with a fan ensuring mixing

213 within minutes. In contrast to the JPAC chamber, the stirring is conducted perpendicular to the cylinder axis, as opposed to

214 coaxial. Chamber inflow is split into two humidified clean air flows (mixed from N_2 and O_2) of about equal volume, one

215 with added oxidant (here O_3), the other with added VOC and other trace gases (here α-pinene and CO). All experiments were

216 performed at a relative humidity of 50 % and at 20 °C. Temperature stability is ensured by the climate-controlled

217 surrounding of the chamber.

218 α-Pinene (≥99 % purity, Sigma-Aldrich Merck KGaA) was introduced via liquid injection with a syringe pump (Fusion
219 4000, CHEMYX Inc.) into a heated glass bulb and flushed by a stream of 1 L min^{-1} into the chamber. CO was added from a
220 gas bottle (10% CO in N_2, Messer SE & Co. KGaA). Ozone was directly produced photolytically before injection with a
221 self-built ozone generator.

222 OH is produced in the chamber by ozone photolysis using two UV-C lamps with a wavelength of 254 nm and subsequent
223 reaction of O(^{1}D) with water vapor. The lamps are mounted in closed quartz cylinders in the middle of the chamber,
224 vertically to the cylinder axis and light intensity can be varied with a movable shielding installed around the lamps. The
225 shielding allows an exact percentage of the lamp to be covered, thus controlling the amount of OH produced in the chamber.

226 The OH radical concentration after CO addition was adjusted by setting the shielding of the UVC lamps and a slight
227 adjustment of O_3 inflow. The applied J(O^{1}D) values in different phases were calculated to be in the range of $0.8 \cdot 10^{-3}$ to
228 $2.4 \cdot 10^{-3}$ s^{-1}.

229 In some of the experiments, ammonium sulfate (≥99 % purity, Merck KGaA) seed particles were added to the system to
230 provide a surface for the condensation of organic material. The aerosol was produced with a modified TSI atomizer (Model
231 3076, TSI GmbH) and dried to 50% relative humidity.

232 VOC concentrations in the chamber were measured using proton-transfer-reaction mass spectrometry (PTR-TOF-MS;
233 Ionicon GmbH). CO_2, CO, H_2O (G2401 Cavity Ringdown Spectrometer, Picarro Inc.), NO, NO_x (NCLD899, Eco Physics
234 GmbH with a home-built photolytic converter) and O_3 (O342e, Envea GmbH) were additionally monitored. Particle
235 distribution and concentration were measured with a condensation particle counter (CPC, Model 3788, TSI GmbH) and a
236 scanning mobility particle sizer (SMPS; Model 3080, TSI GmbH) with a CPC (Model 3788, TSI GmbH). The aerosol
237 composition was measured with a high-resolution aerosol mass spectrometer (HR-TOF AMS; Aerodyne Inc.).

238 In all experiments, VOC, O_3, and SMPS+CPC sampling switched between inlet and outlet of the chamber to measure the
239 input concentrations as well as the concentrations in the reactor. The flow control system of the chamber adapts to these
240 switches so that the inflow into the chamber stays constant.

241 All results discussed here were observed under steady-state conditions when all parameters were constant. For each steady
242 state, the OH concentration was calculated from the decay of α-pinene as described by Kiendler-Scharr et al. (2009).
243 **Equation (5)** is derived from the mass balance of α-pinene at steady state. The steady state OH concentration [OH]$_{SS}$
244 depends on the amount of α-pinene consumed by reaction with OH and the reaction with O_3, as well as the flush out.

$$[OH]_{SS} = \frac{\frac{F}{V} * \frac{[VOC]_{in} - [VOC]_{SS}}{[VOC]_{SS}} - k_{O3} * [O_3]_{SS}}{k_{OH}} \qquad (5)$$

245 Here, F is the total flow and V the volume of the chamber. The subscript "SS" indicates steady-state concentrations, while
246 [VOC]$_{in}$ represents the α-pinene concentration entering the chamber. k_{o3} and k_{OH} represent the reaction rate constants of α-

247 pinene with the corresponding oxidant. We applied rate coefficients of $k_{OH}=5.36\cdot10^{-11}\,cm^3\cdot s^{-1}$ (Atkinson and Arey, 2003) and

248 $k_{O3}=9.25\cdot10^{-17}\,cm^3\cdot s^{-1}$ (Cox et al., 2020) at 20 °C. The uncertainty of the OH calculation was estimated as 20 % by Wildt et

249 al. (2014).

3.2   Experiment conditions

251 An overview of the experiments and their boundary conditions can be found in **Table 1**. Four experiments were performed

252 in total, leading to one repetition of each studied condition. In two of the experiments ammonium sulfate seeds were added

253 leading to a total particle surface in the chamber on the order of $8\cdot10^{-4}\,m^2\,m^{-3}$ and organic loadings of about 3 ug m^{-3} in the

254 photooxidation stage. In the unseeded experiments no significant nucleation was observed leading to pure gas phase

255 conditions. The _Exp2_ experiment is a consecutive combination of a seeded, followed by a non-seeded experiment to provide

256 direct insight into the effect of seed presence on the system.

257 As the OH radical is produced by photolysis of ozone and α-pinene reacts with ozone, it is important to know the relative

258 contribution of the α-pinene consumption by OH and by O_3. This is achieved by comparing the turnover of α-pinene with

259 OH and O_3 respectively. The results can be found in **Table 1**. The listed results are for the low HO_2/RO_2 conditions, but

260 nearly identical values were reached after the HO_2/RO_2 shift.

261 **Table 1. Overview of experimental conditions**

Name	Experiment description	[VOC]$_{in}$	[CO]$_{in}$	[OH]$_{ss}$ at low HO$_2$/RO$_2$	Contribution of OH to turnover at low HO$_2$/RO$_2$	Particle surface at low HO$_2$/RO$_2$	Organic mass concentration at low HO$_2$/RO$_2$
Exp1	_unseeded (1)_	10 ppbv	2.5 ppmv	4.1E+6 cm^{-3}	80 %	-	-
Exp2.1	_seeded (1)_	10 ppbv	2.5 ppmv	1.0E+7 cm^{-3}	91 %	8.7E-4 m^2 m^{-3}	3.4 µg m^{-3}
Exp2.2	_unseeded (2)_	10 ppbv	2.5 ppmv	1.3E+7 cm^{-3}	93 %	-	-
Exp3	_seeded (2)_	10 ppbv	2.5 ppmv	1.4E+7 cm^{-3}	79 %	6.8E-4 m^2 m^{-3}	2.7 µg m^{-3}

262

3.3 Experimental procedure
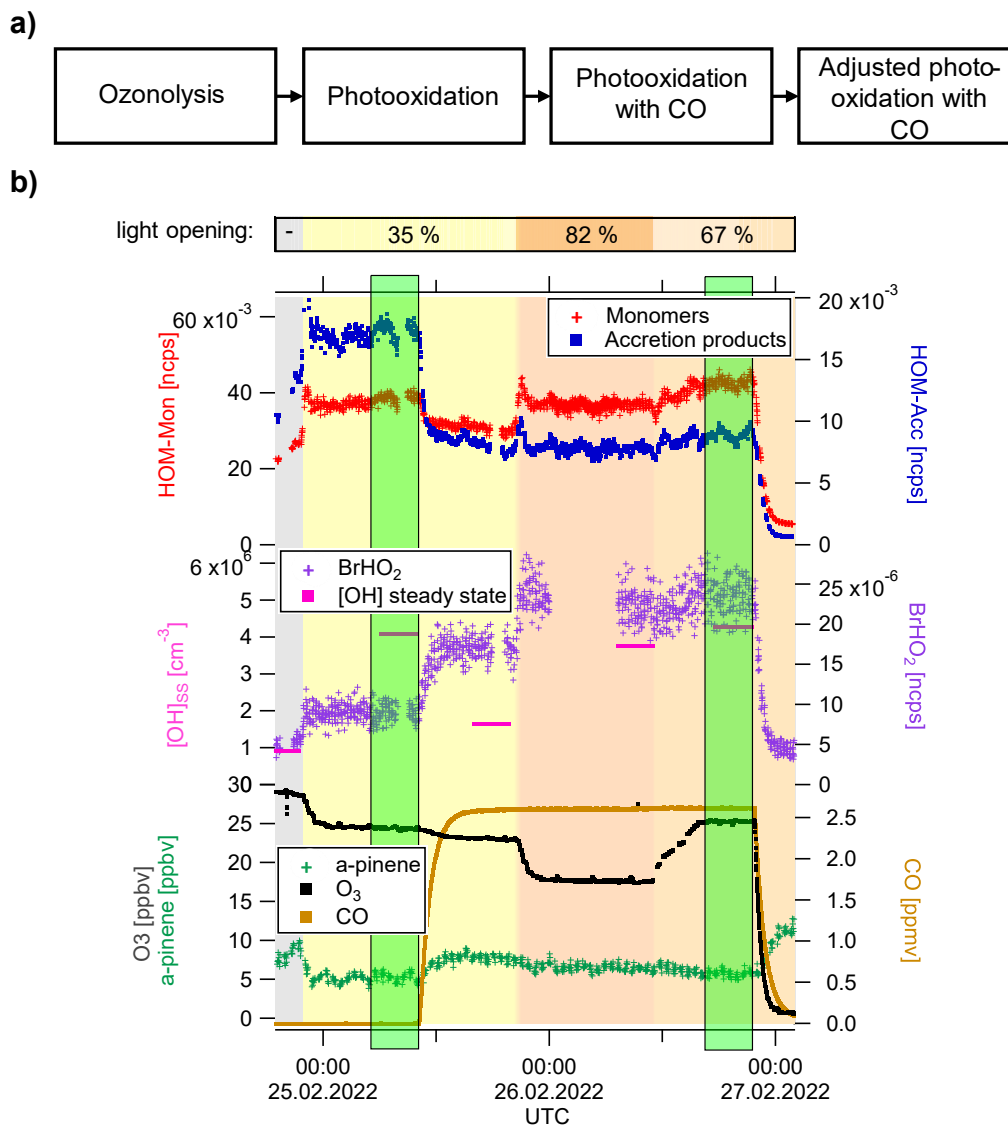
Figure 2: a) Experiment flow scheme b) Exemplary timeseries of _Exp1_ experiment showing HOM-Mon and HOM-Acc product sum (top panel), calculated OH concentration and BrHO$_2$ signal (middle panel), and ozone, α-pinene and CO concentrations (bottom panel). Background color represents light intensity. Highlighted in green are the low HO$_2$/RO$_2$ steady state and the steady state at high HO$_2$/RO$_2$ (addition of CO and adjusted oxidant level).

All experiments started with α-pinene ozonolysis followed by illumination of the UVC-lights to induce the reaction with OH. A general flow scheme of the experiment can be found in **Fig. 2**, together with one exemplary timeseries of the unseeded experiment _Exp1_. After the photooxidation steady state, CO was added to the system. In the displayed _Exp1_ the OH level was adjusted in three steps to approach the same concentration as before the CO addition. First the UVC-light opening was adjusted and then O$_3$ was added, and the UVC-light opening was adjusted again. In some experiments initially

274   the effect of CO on the unchanged system was observed, before the adjustment of OH. In other experiments (*Exp2.2*, *Exp3*)

275   the adjustment of the α-pinene OH turnover via ozone concentration and UVC-light opening were made simultaneously with

276   the CO addition. Highlighted in green are the steady states with the "same" OH concentration characterized by low and high

277   HO_2/RO_2, which were used for analysis and interpretation.

3.4   Model calculation for HO_2/RO_2 ratio estimation

279   Box model calculations were performed applying the MCM v3.3.1 chemistry (Jenkin et al., 1997; Saunders et al., 2003)

280   under the boundary conditions of the SAPHIR-STAR chamber. All calculations were performed with the institute software

281   package EASY which uses FACSIMILE to solve the differential equations (EASY Version 5.69b). More details about the

282   model parameters can be found in the supplement **Sect. S3**. The model calculations reproduced the primary observables

283   α-pinene, O_3, CO, and OH within the experimental uncertainties. The box-model results were used to characterize the

284   HO_2/RO_2 ratio of the chemical systems, as no direct measurement of these parameters was available. The observed cluster

285   signal $BrHO_2^-$ follows the modelled HO_2 concentration (**Fig. 3**).

286   The model predicts a shift of the HO_2/RO_2 ratio from about 0.01 to about 1 by CO addition and oxidant adjustment, an

287   increase by two orders of magnitude. Owing to lack of observations to verify model results, we will consider only the

288   magnitude of HO_2/RO_2 here. The model results show that indeed a major shift from RO_2+RO_2 to RO_2+HO_2 reactions can be

289   expected.

290   We further used the modelled RO_2 and HO_2 concentrations to estimate the relative importance of pathways for individual

291   (observed) HOM-RO2. For that we applied two generic rate coefficients k_{RO2HO2} and k_{RO2RO2}. As the rate coefficient for the

292   RO_2+HO_2 termination to a hydroperoxide k_{RO2HO2} we used the value specified in the MCM ($2.46 \cdot 10^{-11}$ $cm^3 \cdot s^{-1}$ at 20 °C

293   (Jenkin et al., 1997; Saunders et al., 2003)). We chose a k_{RO2RO2} of $5 \cdot 10^{-12}$ $cm^3 \cdot s^{-1}$ as the approximated reaction rate of the

294   RO_2+RO_2 reactions. This value applies to all possible reactions (accretion product, monomer, and alkoxy formation) and is

295   in the range of k_{RO2RO2} utilized by Roldin et al. (2019) in the PRAM model.

3.5   Determination of oxidized VOCs, HOMs and HO_2

297   Chemical ionization mass spectrometry (HR-TOF-CIMS) techniques were used to detect a range of gaseous compounds. For

298   this, two atmospheric pressure interface time of flight mass spectrometers (APi-TOF-MS; Tofwerk AG) with different inlet

299   systems were used simultaneously. General information about the APi-TOF-MS instrument can be found in Junninen et al.

300   (2010).

301   A long TOF (LTOF) (Resolution ~8500 for peaks at >200 m/Q) was coupled with the multi-scheme ionization inlet (MION;

302   Karsa Oy). The setup of the inlet is described in detail by Rissanen et al. (2019). The distinctive feature of the MION inlet is

303   the switching between two reagent ions. Here, nitrate was used to detect closed-shell HOMs, as well as HOM-RO_2. Bianchi

304   et al. (2019) suggested to define HOM as products stemming from autoxidation containing more than 6 oxygen. In our

305 overall analysis we decided to also include fragments and monomers containing 5 or in a few cases 4 oxygens (see peaklist
306 in supplement **Sect. S5**) as we are interested to see if the importance of these less oxidized (but still with NO_3-CIMS
307 detectable) products increases at higher HO_2/RO_2. However, in all considerations regarding SOA formation we furthermore
308 set a molar weight threshold which automatically excluded any products with less 6 oxygens.

309 As the second reagent ion, bromide was used to detect less oxidized products and the HO_2 radical (Albrecht et al., 2019;
310 Sanchez et al., 2016). The nitrate ion source had a reaction time of 600 ms, while the bromide ion source had a shorter
311 reaction time of 60 ms. For all experiments an inlet flow of 10 L min⁻¹ was used and the ionization scheme was switched
312 every 10 minutes.

313 In the data evaluation the first step was the separation of the timeseries of the two reagent ions. The data was subsequently
314 processed with Tofware (Version 3.2.3, Tofwerk AG) using the high resolution timeseries workflow. No transmission
315 correction was performed as previous measurements showed an approximately flat relative transmission curve in the mass
316 region of interest. The analyte signals were normalized with the reagent ion signal (NO_3^- and $HNO_3NO_3^-$ for nitrate and Br^-
317 and BrH_2O^- for bromide).

318 Since no direct HO_2 calibration was available, the HO_2 signal in the Br-MION-CIMS was used to compare the levels of HO_2
319 relative to each other in the different phases of the experiment. The comparison of the measured HO_2 signal to the modelled
320 HO_2 concentration shows a good linear relation between the model predictions and observations.
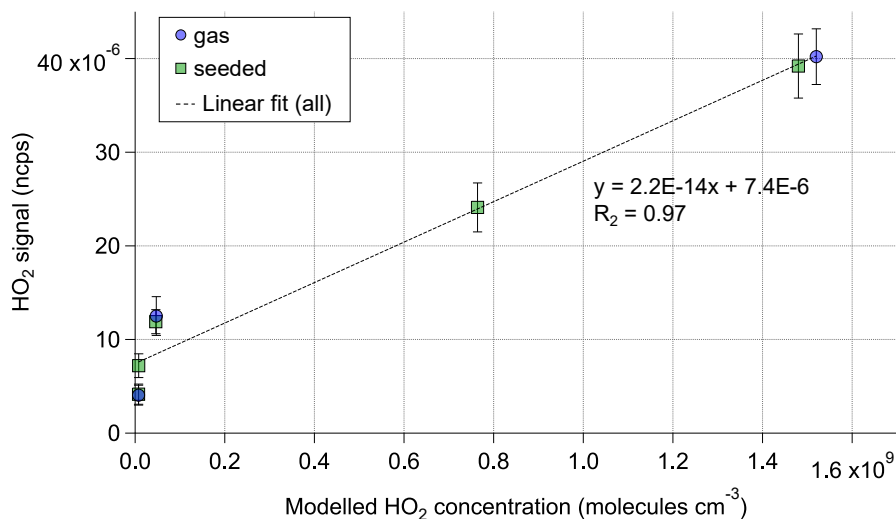
321
322 **Figure 3: Modelled HO_2 concentration vs. normalized HO_2 signal for each steady state of _Exp2_. HO_2 is measured as the $BrHO_2$**
323 **cluster and is normalized with the sum of the reagent ion Br^- and its water cluster. The dotted line shows the linear fit to all (gas**
324 **phase and seeded) measurement points.**

325 **Figure 3** illustrates this for the example of the _Exp2_ experiment. A background signal of around ~$1·10^{-5}$ is observed as soon
326 as VOC and ozone are present in the reactor. The background HO_2 signal was not observed when only O_3 or only VOC were

327 in the system. As shown by the MCM modelling results HO_2 production of this strength is not expected in the α-pinene

328 ozonolysis phase but this background phenomenon was observed before (Albrecht et al., 2019) and is not fully understood.

329 For the HOM molecules measured by the NO_3-MION-CIMS the relative changes between different experiment phases are

330 compared. For all detected HOM products the same detection sensitivity is assumed. Hyttinen et al. (2018) showed in

331 quantum chemical calculations that HOMs containing 6 or more oxygen atoms have comparable sensitivity with the nitrate

332 reagent ion. At this degree of oxidation it can be expected that the HOMs already contain multiple hydroperoxyl and/or

333 hydroxy functional groups (Bianchi et al., 2019) prior to the termination step, making it unlikely that the sensitivity is

334 strongly influenced by the termination group. Thus, the signal strength reflects the correct ranking of the observations and

335 relative comparisons do not require calibration. Pullinen et al. (2020) studied the mass balance between condensable HOMs

336 and formed particle mass and were able to find closure within a factor of 2.

337 A second CI-APi-TOF was used to measure less oxidized species. It was configured with a CI inlet based on the design of

338 Eisele and Tanner (1993) coupled to an HTOF (Resolution ~2700 for peaks at >200 m/Q) (Tofwerk AG) and was operated

339 in positive mode with propylamine ($C_3H_7NH_2$, Sigma-Aldrich, purity ≥99%) to detect the early generation RO_2 and

340 oxidation products (Berndt et al., 2018). The propylamine was purified and added as an amine-N_2 mixture (flow:

341 0.12 mL min^{-1}) to the 30 L min^{-1} sheath flow. Furthermore, the sheath flow air is humidified to optimize ionization. The

342 instrument sampled 0.1 L min^{-1} from the chamber, which was diluted with 9.9 L min^{-1} for a sample flow of 10 L min^{-1}. The

343 dilution was necessary to reduce depletion of the primary ion (Hantschke, 2022).

4 Results and Discussion

345 In order to understand the effect of HO_2/RO_2 on the gas phase product composition, we will present and compare two cases:

346 The steady state without CO (low HO_2/RO_2) and the steady state with CO addition and OH adjustment by $J(O^1D)$ and O_3

347 (high HO_2/RO_2). The modelling results predicted HO_2/RO_2 of about 1/100 and of about 1/1 for these two cases respectively.

348 The modelled concentrations can be found in supplement **Sect. S4**. The modelling results show that the HO_2/RO_2 ratio

349 changes by two orders of magnitude, because [RO_2] was reduced by about a factor of three, while [HO_2] was increased by a

350 factor of 30. Consequently, HO_2 reactions were almost negligible at low HO_2/RO_2 while RO_2+RO_2 reactions can still

351 contribute at high HO_2/RO_2.

352 HO_2/RO_2 ratios of around 1 are highly relevant for atmospheric conditions with significant OH oxidation, though it should

353 be kept in mind that in atmospheric conditions the methyl peroxy radical and other small RO_2 contribute a significant portion

354 to the total of peroxy radicals (Khan et al., 2015). Field studies reporting HO_2 and RO_2 measurements for different

355 environments can be found in supplement **Table S5**. These exemplary studies show that HO_2/RO_2 ratios around 1 are

356 relevant in remote to urban environments with different VOC sources and NO_x levels.

357 Assuming correctly modelled [HO$_2$] and [RO$_2$], we calculated the competition between HO$_2$ and RO$_2$ reactions for each

358 (observed) RO$_2$ expressed in form of pseudo first order rate coefficients in k$_{RO_2HO_2}$ · [HO$_2$] or k$_{RO_2RO_2}$ · [RO$_2$]. Herein

359 [RO$_2$] is the sum of all RO$_2$ species as defined in the MCM v3.3.1. For all experiments the results of our calculations indicate

360 that the sink for HOM-RO$_2$ is dominated by RO$_2$+RO$_2$ reactions at low HO$_2$/RO$_2$ (~97 % contribution), while at high

361 HO$_2$/RO$_2$ RO$_2$+HO$_2$ contributed ~75 %. As the rate coefficients are not well known and we cannot verify the modelling

362 results for HO$_2$ and RO$_2$ our calculations serve solely as an indication of expected trends in the chemical system.

4.1 Impact on overall HOM-formation

364 The top panel of **Fig. 2** shows the timeseries of HOM-Mon and HOM-Acc products. The HOM-Mon signal recovers after

365 the oxidant adjustment, while the HOM-Acc signal is significantly suppressed at high HO$_2$/RO$_2$. This indicates that the shift

366 from low to high HO$_2$/RO$_2$ substantially impacts the termination reactions, shifting formation from the HOM-Acc product

367 channel (RO$_2$+RO$_2$) to the HOM-Mon channel.

368 An overview of the results for the product classes defined in the method section is shown in **Fig. 4**. Plotted are the average

369 ratios of signal in the NO$_3$-CIMS in the high HO$_2$/RO$_2$ steady state compared to the low HO$_2$/RO$_2$ steady state. For better

370 comparison, all experiment phases were normalized to the actual α-pinene OH turnover. The overall HOM-signal was lower

371 at high HO$_2$/RO$_2$ showing a reduction of about 20 %. Most distinctive, the HOM-Acc were strongly reduced by about 60 %.

372 A reduction of HOM-Acc by addition of CO was observed before by McFiggans et al. (2019), however there the OH

373 concentration was not kept constant. The HOM-Frag (5≥C<10) also show a reduction of about 20 %. At high HO$_2$/RO$_2$

374 C$_{10}$-HOM-RO$_2$ were also reduced significantly by about 40 %.
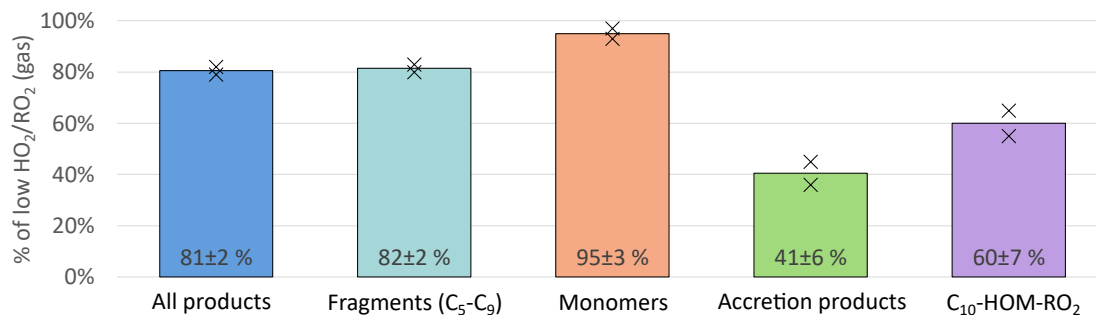
375

376 **Figure 4: Overview of average, relative change in product classes detected in NO$_3$-CIMS between low and high HO$_2$/RO$_2$ case**
377 **(both normalized to α-pinene OH turnover) for unseeded experiments. Bars represent average of the two experiments, markers**
378 **represent individual experiments.**

379 The HOM-Mon signal level remained about the same at low and high HO$_2$/RO$_2$. Without changes in the rates and

380 contributions of the different termination reactions, the observed reduction in the HOM-RO$_2$ precursors should lead to nearly

381 the same reduction in HOM-Mon. However, the decrease of accretion product formation and fragmentation should lead to an

382 increase in HOM-Mon. The presence of HO$_2$ could reduce the alkoxy formation, and thus fragmentation of HOM-RO$_2$. This

383 missing sink could lead to an additional HOM-Mon source compared to the low HO_2/RO_2 case. However, the distribution of

384 the product classes at low and high HO_2/RO_2 (**Fig. 5**) shows that contributions are shifted from HOM-Acc to HOM-Mon,

385 while the contribution of HOM-Frag remains constant. Each HOM-Acc is formed from one HOM-RO_2 (HOM-RO_2+RO_2) or

386 potentially even two HOM-RO_2 (HOM-RO_2+HOM-RO_2) and therefore each HOM-Acc not formed will lead to at least one

387 HOM-Mon.
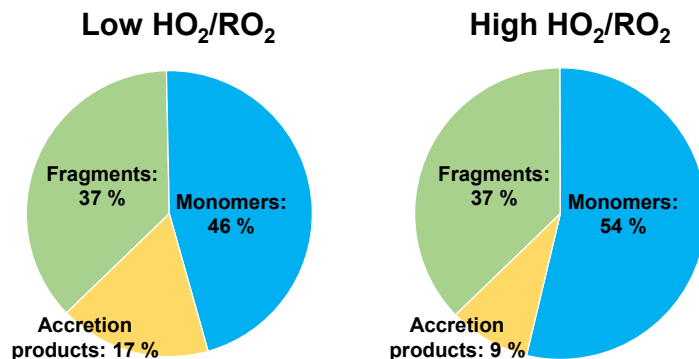
388

389 **Figure 5: Average contribution of the closed shell product classes to overall HOM-product signal in the low and high HO_2/RO_2**
390 **cases (unseeded experiments).**

391 Further changes in the product distribution become evident when considering the individual HOM-Mon families as shown in

392 **Fig. 6**. The $C_{10}H_{15}O_x$ peroxy radical family and the related $C_{10}H_{14}O_z$ family (carbonyl compounds) show the strongest

393 suppression with a decrease of about 40 % at high HO_2/RO_2. For the $C_{10}H_{17}O_x$ peroxy radical family the suppression was

394 less pronounced with a 17 % reduction. In contrast, the $C_{10}H_{16}O_z$ family remained about the same while the $C_{10}H_{18}O_z$ family

395 showed a strong increase at high HO_2/RO_2.
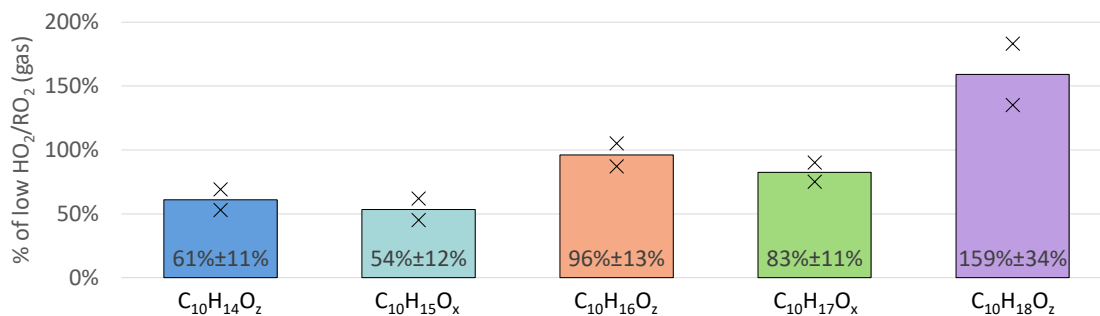
396

397 **Figure 6: Overview of average, relative change in monomer families detected in NO_3-CIMS between low and high HO_2/RO_2 case**
398 **(both normalized to α-pinene OH turnover) for unseeded experiments. Bars represent average of the two experiments, markers**
399 **represent individual experiments.**

400 The suppression of C_{10}-HOM-RO_2 of only about 40 % compared to the reduction of overall [RO_2] by ~70 % in the model

401 calculations (for the modelled concentrations see supplement **Sect. S4**) shows that in many instances the autoxidation is too

402 efficient to be out-competed by the RO_2+HO_2 termination reaction, which is several times faster than RO_2+RO_2 reactions.

403 Furthermore, the signal weighted O/C ratio of the monomer class does not change between low and high HO_2/RO_2 (0.70±

404 0.01). If the HO_2 termination would interrupt the autoxidation chain, a lower oxidation level would be expected at high

405 HO_2/RO_2. The unchanged oxidation level and the suppression of HOM-Acc, indicate that the average autoxidation rate must

406 be faster than $k_{RO2HO2}\cdot[HO_2]$, while the average accretion rate for $k_{HOM-RO2+RO2}\cdot[RO_2]$ must be slower. In conclusion, the

407 change in HO_2/RO_2 should essentially impact the distribution of the HOM-RO_2 termination products.

4.2   Impact on HOM-RO$_2$

409 C_{10}-HOM-RO_2 are key to understand the changes in the HOM product distribution. Therefore, we will first discuss the

410 changes in the HOM-RO_2 and then the changes in the closed shell products.

411 The C_{10} peroxy radical class consists of the $C_{10}H_{15}O_x$ and $C_{10}H_{17}O_x$ families which were reduced to 54 % and 83 %,

412 respectively when comparing the high and low HO_2/RO_2 cases (**Fig. 6**, light blue and green bars). The observed reduction in

413 C_{10}-HOM-RO_2 is significantly smaller than the overall RO_2 concentration reduction predicted by the MCM model results

414 (reduction to ~30 %). In the following paragraphs, we present a plausibility consideration to assess if these observed changes

415 are consistent with our expectations from modelling results and reaction rates.

416 The change in the steady state concentration of a compound is always defined by the changes in its sources and sinks. The

417 source of a HOM-RO_2 is the intramolecular reaction of a precursor RO_2 and thus the HOM-RO_2's source is reduced if the

418 steady state concentration of the precursor RO_2 is reduced. However, assuming the source term of the precursor RO_2 is the

419 same in low and high HO_2/RO_2 (due to the constant α-pinene OH turnover) and the precursor RO_2's sink term is dominated

420 by the fast autoxidation in both cases, then the RO_2's steady state concentration would not be significantly changed. This

421 consideration is only applicable for RO_2 where autoxidation dominates the sink term at low and high HO_2/RO_2. However,

422 the unchanged oxidation level of the HOM-Mon indicates that once the autoxidation is initiated it out-competes the possible

423 termination reactions.

424 In this case, the change in steady state concentration of the HOM-RO_2 will be defined by the changes in the sink terms.

425 Owing to the faster reaction of RO_2+HO_2 compared to RO_2+RO_2 the chemical sink for all RO_2 including HOM-RO_2 with

426 slower autoxidation rates increased, which leads to a reduction in the steady state concentration of RO_2 in general, despite

427 holding the primary RO_2 source term constant.

428 For steady state conditions, we can estimate the expected effect on the RO_2 ratio between high and low HO_2/RO_2 conditions

429 for those HOM-RO_2 with production directly linked to the primary production ($k_{OH}\cdot[OH]\cdot[α-pinene]$) with negligible further

430 autoxidation. The necessary equations and assumptions can be found in supplement **Sect. S7.** We assume the same primary

431 production at low and high HO_2/RO_2 and that the reaction with HO_2, the reaction with RO_2 and the wall loss are the only

432 significant loss pathways. At high HO_2/RO_2, a reduction to 80 % is expected if the chosen bulk rate constants are used

433 (k_{RO2HO2}=2.46·10^{-11} cm^3·s^{-1} at 20 °C (Jenkin et al., 1997; Saunders et al., 2003), k_{RO2RO2}=5.0·10^{-12} cm^3·s^{-1}). A reduction to

434 60 % is expected if k_{RO2HO2} is around 7 times faster than k_{RO2RO2} (k_{RO2RO2}=3.3·10^{-12} $cm^3 \cdot s^{-1}$). These reductions are in the range

435 of what is observed for the C_{10}-HOM-RO_2. Of course, the approach of using generalized bulk rate constants is limited, but

436 the resulting values for k_{RO2RO2} were clearly within the range of rate coefficients expected for HOM-RO_2+RO_2 reactions

437 (Roldin et al., 2019) showing that the increased chemical sink is a plausible explanation for our observations.

438 The $C_{10}H_{15}O_x$ family is on average reduced by around 30 % more than the $C_{10}H_{17}O_x$ family (see **Fig. 6**). $C_{10}H_{15}O_X$ peroxy

439 radicals are either formed by sequential oxidation of α-pinene , e.g. from oxidation products like pinonaldehyde, or directly

440 from α-pinene via the H-abstraction pathway (Shen et al., 2022). Formation of pinonaldehyde and, even more so HOM

441 formation via the H-abstraction channel, involve alkoxy steps. However, alkoxy radicals should be reduced at high HO_2/RO_2

442 since they are mainly formed by RO_2+RO_2 reactions in the absence of NO_x. Thus, missing source terms add to the increased

443 chemical sink by HO_2 for $C_{10}H_{15}O_X$ peroxy radicals.

444 Amine CIMS measurements enabled detection of the formula composition $C_{10}H_{16}O_2$ (e.g. pinonaldehyde). $C_{10}H_{16}O_2$ was

445 reduced on average to 71%±1 % at high HO_2/RO_2 compared to low HO_2/RO_2. This supports that a fraction of the $C_{10}H_{15}O_x$

446 radical decrease at high HO_2/RO_2 arose from suppression of $C_{10}H_{16}O_2$ first generation products. In addition, a further

447 suppression of HOM formation via the H-abstraction channel is likely. It should be noted that the reduction of $C_{10}H_{16}O_2$ is

448 smaller than that expected by the MCM model results. Modelling results can be found in supplement **Sect. S4**. This might

449 indicate that HO_2 can also enable alkoxy radical steps to a certain degree as summarized by Jenkin et al. (2019) and

450 postulated by e.g. Eddingsaas et al. (2012) as a source of pinonaldehyde in HO_2 dominated systems.

451 According to the model calculations the pseudo first order rate coefficient $k_{RO2HO2} \cdot [HO_2]$ is expected to be about 0.03 s^{-1} for

452 the RO_2+HO_2 reaction at high HO_2/RO_2. Consequently, only such HOM-RO_2 with autoxidation rates of ≤0.03 s^{-1} will be

453 significantly lost by reaction with HO_2 at the higher HO_2 concentrations. However, typical isomerization rates of peroxy

454 radicals in autoxidation are of the order of 0.1 s^{-1} and many are faster (Piletic and Kleindienst, 2022; Berndt, 2021).

455 Therefore, reduction in a HOM-RO_2 is only expected when the faster termination rate of $k_{RO2HO2} \cdot [HO_2]$ can compete with the

456 autoxidation rate, i. e. when the autoxidation slows as the degree of oxidation increases on the specific HOM-RO_2. This

457 consideration shows that the smaller reduction in HOM-RO_2 compared to the lower oxidized RO_2 in the model is compatible

458 with fast autoxidation reactions that are missing in the MCM.

459 The increase in chemical sink strength by going from RO_2 termination to HO_2 termination is the main expected reason for

460 the decrease in $C_{10}H_{17}O_x$. As discussed, the $C_{10}H_{15}O_X$ family is subject to an additional decrease in the precursors due to the

461 alkoxy steps necessary in the formation pathway. Since $C_{10}H_{15}O_X$ were the main contributors to the C_{10}-HOM-RO_2 class

462 their stronger reduction is reflected in the overall reduction of C_{10}-HOM-RO_2.

4.2.1 Contribution of $C_{10}H_{15}O_x$ and $C_{10}H_{17}O_x$ families to HOM-RO$_2$

In the unseeded, pure gas phase experiments, the contribution of the $C_{10}H_{17}O_x$ family to the C_{10}-HOM-RO$_2$ class is 23 % ±2 % on average in the low HO$_2$/RO$_2$ case. In the high HO$_2$/RO$_2$ case the contribution increases to 31 % ±4 % on average. As discussed above the suggested pathways to $C_{10}H_{15}O_x$ HOM-RO$_2$ may be additionally suppressed due to a decrease of alkoxy steps at high HO$_2$/RO$_2$ reducing the entry channel into $C_{10}H_{15}O_x$ HOM-RO$_2$.

Nevertheless, the contribution of $C_{10}H_{15}O_x$ is substantial in both experiment stages. Kang (2021) and Shen et al. (2022) reported that, in the photooxidation of α-pinene, the HOM-RO$_2$ detected by NO$_3$-CIMS are dominated by the $C_{10}H_{15}O_x$ family, while $C_{10}H_{17}O_x$ formation is the main expected OH reaction pathway described in literature (Berndt, 2021; Berndt et al., 2016; Xu et al., 2019).

This hints towards an effective pathway to HOM via $C_{10}H_{15}O_x$. A reason may be the fast opening of both carbon-rings in the bicyclic α-pinene (Shen et al., 2022), or a four-ring opening in pinonaldehyde or similar compounds, for easy autoxidation. From our observations increasing the HO$_2$/RO$_2$ ratio does increase the relative importance of the $C_{10}H_{17}O_x$ family, but the change is less than 10 % in contribution.

Contribution of the two peroxy radical families to the HOM formation is also reflected in the composition of C_{20} HOM-Acc. **Figure 7** shows the average contributions of the $C_{20}H_{30}O_z$, $C_{20}H_{32}O_z$, and $C_{20}H_{34}O_z$ families in the low and high HO$_2$/RO$_2$ cases. Although the absolute amount of HOM-Acc was suppressed by 60 % the family distribution was similar, $C_{20}H_{32}O_z$ dominated, while $C_{20}H_{30}O_z$ was lowest. $C_{20}H_{30}O_z$ is formed from two members of the $C_{10}H_{15}O_x$ family, while $C_{20}H_{34}O_z$ is formed by two members of the $C_{10}H_{17}O_x$ family. $C_{20}H_{32}O_z$ is then a combination of a $C_{10}H_{15}O_x$-RO$_2$ and $C_{10}H_{17}O_x$-RO$_2$.

Families that require one or two $C_{10}H_{17}O_x$ peroxy radicals for their formation have a higher contribution than the $C_{10}H_{17}O_x$ family's contribution to C_{10}-HOM-RO$_2$. Here, it is important to note that not only HOM-RO$_2$ can participate in HOM-Acc formation, but also traditional, less oxidized RO$_2$ radicals (Berndt et al., 2018; Pullinen et al., 2020; McFiggans et al., 2019), which are not detectable by NO$_3^-$-CIMS. However, more oxidized peroxy radicals exhibit faster accretion rates (Berndt et al., 2018).
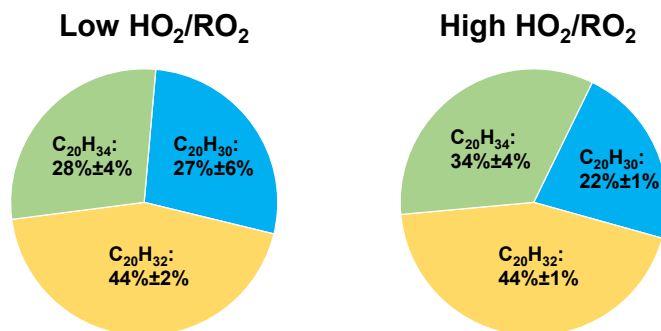
Figure 7: Average contribution of the $C_{20}H_{30}O_z$, $C_{20}H_{32}O_z$, and $C_{20}H_{34}O_z$ family to the C_{20} HOM-Acc group signal in the low and high HO_2/RO_2 cases (unseeded experiments). Not pictured is $C_{20}H_{28}O_z$ due to its negligible signal (contribution ~1 %).

The large contributions of $C_{20}H_{32}O_z$ and $C_{20}H_{34}O_z$ thus clearly show the general importance of the $C_{10}H_{17}O_X$ peroxy radicals. The largest fraction, the $C_{20}H_{32}O_z$ family indicates the importance of HOM-$C_{10}H_{15}O_x$ and a high abundance of lower oxidized $C_{10}H_{17}O_X$ peroxy radicals. Lower oxidized $C_{10}H_{17}O_X$-RO_2 were recently measured by Berndt (2021). The fraction of $C_{20}H_{34}O_z$ is smaller because their formation requires HOM-$C_{10}H_{17}O_X$ radicals which are less abundant compared to HOM-$C_{10}H_{15}O_x$, while the small fraction of $C_{20}H_{30}O_z$ indicates that, despite the importance of HOM-$C_{10}H_{15}O_x$, lower oxidized $C_{10}H_{15}O_x$ are less important.

These results indicate the importance of mixed HOM-Acc formation by cross reactions of HOM-RO_2 and a lower oxidized RO_2. The importance of mixed HOM-Acc is supported by the relatively small fractions of HOM-Acc products with very high oxygen numbers, which more likely stem from HOM-RO_2+HOM-RO_2. For example, C_{20}-HOM-Acc with 12 or more oxygen atoms contribute only around 30 % (low HO_2/RO_2: 26 % ±4 %, high HO_2/RO_2: 31 % ±2 %) of the signal in the product group.

Although the effect of the changed HO_2/RO_2 ratio is small, a tendency to higher $C_{20}H_{34}O_z$ contribution was observed. This is consistent with the observation of a slightly higher $C_{10}H_{17}O_x$ contribution to the C_{10}-HOM RO_2. The stronger suppression of the $C_{10}H_{15}O_x$ family at high HO_2/RO_2 is the first indication for, and can be explained by, a reduction in the alkoxy radical formation.

4.2.2 Impact on HOM-Alkoxy radical formation

Alkoxy radicals (RO) are the second important radical type in the oxidation chain of α-pinene. RO cannot be detected directly as they are highly unstable and thus have very low concentrations. However, as explained in **Sect. 2.2** the parity change in the HOM-RO_2 families can be used as a diagnosis tool for the abundance of alkoxy steps (Kang, 2021). A second indicator for alkoxy steps is the abundance of HOM products with less than 10 C-atoms.

Figure 8 shows the average contribution of $C_{10}H_{15}O_x$ and $C_{10}H_{17}O_x$ with an even and odd number of oxygens at low and high HO_2/RO_2. $C_{10}H_{15}O_x$ radicals with an even number of oxygens contribute on average 32 % at low HO_2/RO_2. For $C_{10}H_{15}O_x$, the autoxidation chain is expected to start from an even number of oxygen either from $C_{10}H_{15}O_4$ (pinonaldehyde-like) (MCM v3.3.1 (Jenkin et al., 1997; Saunders et al., 2003) or from $C_{10}H_{15}O_2$ ($C_{10}H_{16}$ H-abstraction) (Berndt, 2021; Shen et al., 2022). Therefore, without the involvement of an alkoxy step, the parity of the oxygen number in the observed $C_{10}H_{15}O_x$ HOM-RO_2 is expected to be even. Due to the average contribution of $C_{10}H_{15}O_{odd}$ of 69 % we conclude that at least one alkoxy step (or any odd number of alkoxy steps) must have taken place in most of the cases at low HO_2/RO_2.

516
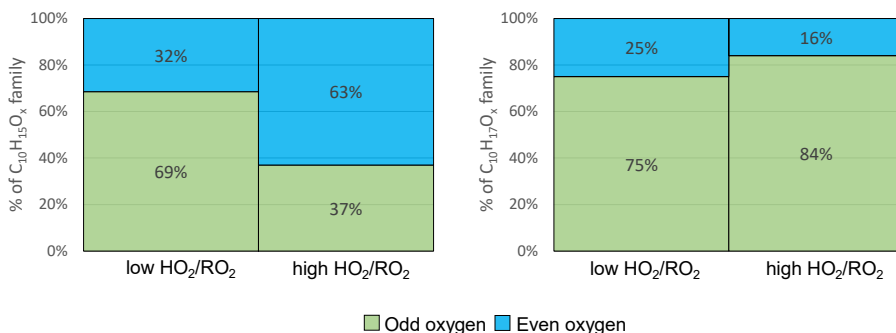
Figure 8: Average contribution of O_{odd} and O_{even} to the HOM-RO$_2$ families $C_{10}H_{15}O_x$ (left) and $C_{10}H_{17}O_x$ (right) signal in the low and high HO$_2$/RO$_2$ cases (unseeded experiments).

At high HO$_2$/RO$_2$ $C_{10}H_{15}O_{even}$ contributed 63 % and the $C_{10}H_{15}O_{odd}$ contribution was reduced to 37 %. This demonstrates a change in the number of alkoxy steps along the formation pathway of the observed HOM-RO$_2$ radicals. The increased contribution of $C_{10}H_{15}O_{even}$ at high HO$_2$/RO$_2$ lets us infer an even number of alkoxy steps as more common (0,2,4…). In the simplest case 1 alkoxy step takes place at low HO$_2$/RO$_2$ due to HOM-RO formation from HOM-RO$_2$+RO$_2$ reactions, while no alkoxy step takes place at high HO$_2$/RO$_2$, because HOM-RO$_2$+HO$_2$ produces none or less HOM-RO than HOM-RO$_2$+RO$_2$.

For $C_{10}H_{17}O_x$ the entry channel into autoxidation is $C_{10}H_{17}O_3$ with an odd number of oxygen atoms. Therefore, in autoxidation without alkoxy steps the oxygen parity is expected to be odd. At low HO$_2$/RO$_2$ $C_{10}H_{17}O_{odd}$ species contribute 75 % to the total $C_{10}H_{17}O_x$ signal indicating that either none or an even number (2,4,…) of alkoxy steps occurred. At high HO$_2$/RO$_2$ the odd contribution increases to 84 % (see **Fig. 8**). This result could indicate a low occurrence of alkoxy steps even at low HO$_2$/RO$_2$, with a further decrease of alkoxy formation at high HO$_2$/RO$_2$. However, the observed shift is minor.

In any case the different responses of the $C_{10}H_{15}O_x$ and $C_{10}H_{17}O_x$ families to the reduction of HOM-RO$_2$ formation from HOM-RO$_2$+RO$_2$ at high HO$_2$/RO$_2$ indicate that there could be fundamental differences in the autoxidation chains of $C_{10}H_{15}O_x$ and $C_{10}H_{17}O_x$ (or the limit of the parity analysis). The parity analysis indicates a decrease in alkoxy steps at high HO$_2$/RO$_2$, but it cannot be directly inferred with certainty. However, decrease in alkoxy steps at high HO$_2$/RO$_2$ is supported by the observation of changes in HOM-Frag products.

On average the sum of all HOM-Frag products (detected compounds with $5 \geq C < 10$ by NO$_3^-$-CIMS) showed a reduction of around 20 % (unseeded experiments, see **Fig. 4**). Further trends become recognizable when separating the species according to their carbon number. **Figure 9** shows the C_5, C_7, C_8, and C_9 HOM-Frag at high HO$_2$/RO$_2$ compared to the low HO$_2$/RO$_2$ case, normalized to the α-pinene OH turnover. The fragment group with C_6 compounds is not included, as it contributed less than 5 % of the fragment signal and contained few detected compounds.
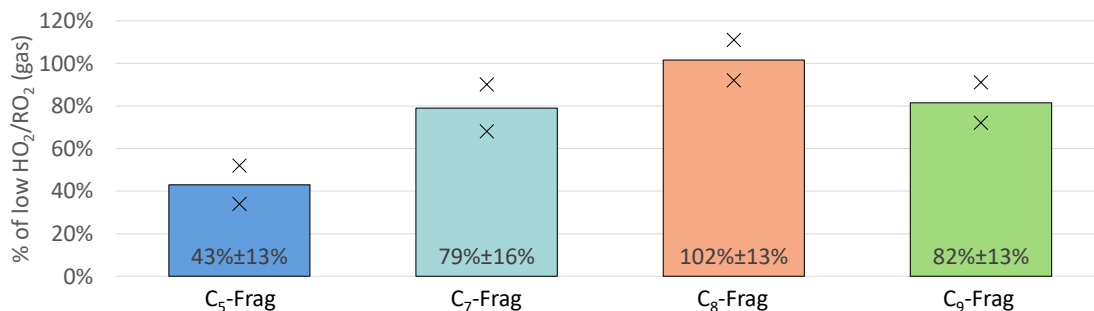
540

541 **Figure 9: Overview of average, relative change in C_5, C_7, C_8, C_9 fragment groups detected in NO₃-CIMS between high and low**
542 **HO_2/RO_2 case (both normalized to α-pinene OH turnover) for unseeded experiments. Bars represent average of the two**
543 **experiments, markers represent individual experiments.**

544 **Figure 9** shows a significant reduction in HOM-Frag with shorter carbon chain length: C_5 HOM-Frag are reduced by around

545 60 % compared to the low HO_2/RO_2 case. If we assume that the fragmentation of C_{10} compounds happens in consecutive

546 steps via scission of HOM-RO radicals (analogously to the MCM), this observation is in accord with decreasing importance

547 of alkoxy radical formation at high HO_2/RO_2.

548 Overall, all observations indicate strong involvement of RO in HOM formation as well as a reduced, but still significant,

549 involvement of RO at high HO_2/RO_2, when HO_2 chemistry dominates: This is supported by the change of the oxygen parity

550 in C_{10}-HOM-RO_2, and the decrease of fragmentation products, especially with lower carbon number, as well as the only

551 moderate reduction in the observed $C_{10}H_{16}O_2$ product (pinonaldehyde) and the still substantial importance of the $C_{10}H_{15}O_x$

552 HOM-RO_2 family at high HO_2/RO_2.

4.3 Impact on carbonyl and hydroperoxide formation

554 Increased HO_2/RO_2 should shift the product distribution by reduction of alcohol and carbonyl compounds from the so-called

555 molecular channel in the RO_2+RO_2 reaction (see reaction (*R3*)), in favor of hydroperoxide formation from RO_2+HO_2

556 termination (reaction (*R1*)). This effect can be best observed in the $C_{10}H_{18}O_z$ family, which contains the hydroperoxide and

557 alcohol termination products arising from $C_{10}H_{17}O_x$. $C_{10}H_{18}O_z$ significantly increased to on average 159 % (see **Fig. 6**). This

558 supports an increased hydroperoxide formation, however, with some uncertainty due to the alcohol termination products

559 from $C_{10}H_{17}O_x$ (by reaction with RO_2). To elucidate this further the contribution of individual species to the $C_{10}H_{18}O_z$ family

560 was examined.

561 Formation of an alcohol via the molecular path (reaction (*R3*)) leads to the loss of one oxygen atom compared to the

562 precursor $C_{10}H_{17}O_x$ radical, while in the hydroperoxide formation (reaction (*R1*)) the oxygen number remains the same. The

563 most abundant member of the $C_{10}H_{17}O_x$ family was $C_{10}H_{17}O_7$ with a contribution of 72 % ±6 % at low HO_2/RO_2, and a

564 contribution of 82 % ±1 % at high HO_2/RO_2. $C_{10}H_{17}O_7$ terminates to $C_{10}H_{18}O_z$ products either as an alcohol with sum

565 formula $C_{10}H_{18}O_6$, or as a hydroperoxide with sum formula $C_{10}H_{18}O_7$. These products have additional sources from $C_{10}H_{17}O_6$

566 and $C_{10}H_{17}O_8$ but due to the dominant contribution of $C_{10}H_{17}O_7$ to the $C_{10}H_{17}O_x$ family we expect any other production

567 channels to be of minor importance.

568 **Figure 10** shows the HOM product distribution within the $C_{10}H_{18}O_z$ family at low and high HO_2/RO_2. The sum of the O_6 and

569 O_7 product did not change significantly in the two regimes (about 88 %), showing that these are the major products, and

570 agreeing well with the observation of $C_{10}H_{17}O_7$ being the major $C_{10}H_{17}O_x$ HOM-RO_2. At low HO_2/RO_2 the O_6 product has a

571 larger contribution of 64 %±8 %, while at high HO_2/RO_2 ~30 % of signal is shifted to the O_7 product. This shows that the

572 increase in the $C_{10}H_{18}O_z$ is matched with an increase of hydroperoxide formation.
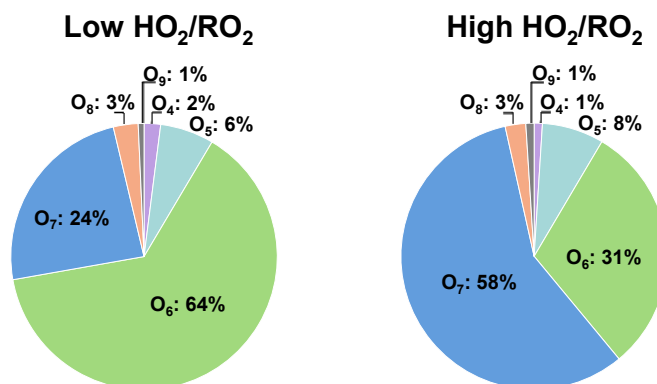
573

574 **Figure 10: Average contribution of the individual compounds to the $C_{10}H_{18}O_z$ family signal at low and high HO_2/RO_2 (unseeded**
575 **experiments).**

576 An indicator for carbonyl formation is the $C_{10}H_{14}O_z$ family as it only contains the carbonyl products arising from

577 $C_{10}H_{15}O_x$-RO_2. The $C_{10}H_{14}O_z$ family was reduced on average to 61 % at high HO_2/RO_2, however this decrease matches the

578 decrease in the $C_{10}H_{15}O_x$ precursor family. If the reaction of a $C_{10}H_{15}O_x$-HOM-RO_2 with a second RO_2 were the main

579 formation pathway for $C_{10}H_{14}O_z$ a stronger reduction would be expected as both precursor species were decreased

580 significantly. Instead, it appears that $C_{10}H_{14}O_z$ is mainly impacted by the decrease in $C_{10}H_{15}O_x$ as their reductions are similar.

581 A possible explanation could be that intramolecular termination is a major reaction pathway for $C_{10}H_{15}O_x$-RO_2, forming

582 $C_{10}H_{14}O_x$-carbonyls. Intramolecular termination of the autoxidation chain has been discussed in the literature for different

583 VOCs (Shen et al., 2021; Guo et al., 2022), Rissanen et al. (2014) discussed the possible importance of the unimolecular

584 termination via an H-shift, followed by formation of a carbonyl functional group and OH loss in the autoxidation chain of

585 cyclohexene. Piletic and Kleindienst (2022) calculated fast reaction rate constants in the range of 1-30 s^{-1} for such

586 intramolecular termination reactions to carbonyls for some $C_{10}H_{17}O_5$ in the α-pinene photooxidation, indicating that this

587 pathway could also be significant for $C_{10}H_{15}O_x$. However, more investigation is necessary.

588 The overall contributions of the $C_{10}H_{14}O_z$, $C_{10}H_{16}O_z$, and $C_{10}H_{18}O_z$ families to the HOM-Mon class at high HO_2/RO_2 are

589 shifted as shown in **Fig. 11**.

Low HO$_2$/RO$_2$ **High HO$_2$/RO$_2$**

590
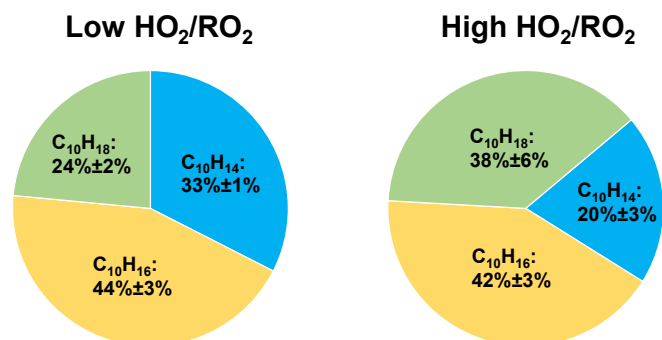
Figure 11: Average contribution of the C$_{10}$H$_{14}$O$_z$, C$_{10}$H$_{16}$O$_z$, and C$_{10}$H$_{18}$O$_z$ family to the monomer class signal at low and high
HO$_2$/RO$_2$ (unseeded experiments).

593 The contribution of C$_{10}$H$_{16}$O$_z$ is largest and remains similar in both cases, matching the already shown unchanged signal
594 level in **Fig. 6**. This is the case because the C$_{10}$H$_{16}$O$_z$ family contains the alcohols from C$_{10}$H$_{15}$O$_x$+RO$_2$, carbonyls from
595 C$_{10}$H$_{17}$O$_x$+RO$_2$ and hydroperoxides from C$_{10}$H$_{15}$O$_x$+HO$_2$ (see **Fig. 1**). A separation of the effects of enhanced HO$_2$ on this
596 monomer family is difficult, as for the case where RO$_2$ termination dominates vs. the case where HO$_2$ termination dominates,
597 the loss of carbonyls and alcohols is partially compensated by the gain of hydroperoxides. A strong gain in hydroperoxides is
598 clearly reflected in the strong increase of C$_{10}$H$_{18}$O$_z$ at high HO$_2$/RO$_2$.

599 Inspection of the C$_{10}$H$_{14}$O$_z$ and C$_{10}$H$_{18}$O$_z$ families shows that ~13 % of the contribution by C$_{10}$H$_{14}$O$_z$ are lost (carbonyls,
600 33 % at low HO$_2$/RO$_2$) and are present instead as C$_{10}$H$_{18}$O$_z$ (hydroperoxides), giving C$_{10}$H$_{18}$O$_z$ a contribution of 38 % at high
601 HO$_2$/RO$_2$.

602 **4.4   Impact on condensable organic mass**

603 In the previous sections we demonstrated a shift of the product distribution by the shift from low to high HO$_2$/RO$_2$
604 conditions. We also showed that the changes could be rationalized by generic mechanistic considerations. We added
605 (NH$_4$)$_2$SO$_4$ seed aerosol in two experiments to determine how the shift in the product distribution affects the condensable
606 organic mass by determining the fraction which remained in the gas-phase after seeding.

607 **Figure 12** shows the fraction remaining for the sum of all products as well as for the individual product classes for the high
608 and the low HO$_2$/RO$_2$ case. In both cases a significant reduction of products in the gas phase was observed with seed present.
609 Overall, the sum of all products was reduced by around 60 %, with a slightly higher reduction in the low HO$_2$/RO$_2$ case. This
610 can be attributed to the larger importance of HOM-Acc in the low HO$_2$/RO$_2$ case, as well as to a 10 % lower reduction of the
611 HOM-Frag in the high HO$_2$/RO$_2$ case. In both cases a reduction of the HOM-RO$_2$ is observed, which indicates that the
612 provided particle sink could have affected HOM formation chemistry, however only moderately.
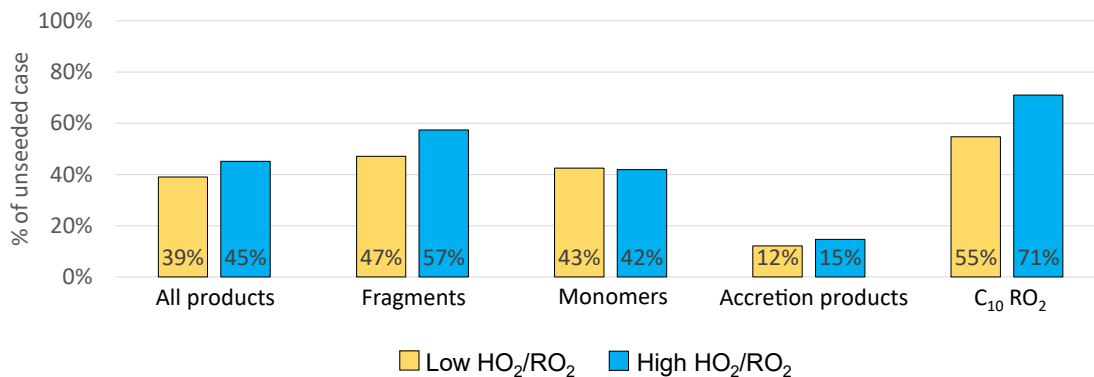
Figure 12: Overview of average, relative change in product classes signal between gas phase only and seeded system. Blue shows the high HO₂/RO₂ case, yellow the low HO₂/RO₂ case. (All are normalized to α-pinene OH turnover, _Exp2_ experiment)

The total organic particulate mass was determined by AMS measurements and was $2.0 \; \mu g \; m^{-3}$ and $3.4 \; \mu g \; m^{-3}$ at high and low HO_2/RO_2 in the experiment (_Exp2_) displayed in **Fig. 12**. A reduction of condensed organic mass to 73 %±3 % at high HO_2/RO_2 (orange bar in **Fig. 14**) was observed on average. Since non-seeded and seeded experiments were conducted at otherwise the same conditions and we did not observe significant new particle formation, the gas-phase compositions can be directly compared. Therefore, we conclude that the shift in the product distribution led to a reduction of condensable material at the same α-pinene turnover with OH (and O_3).

We calculated the wall loss corrected SOA yields with the corrected SOA mass as shown in **Eq. (4)** and as described by Sarrafzadeh et al. (2016). To this end we used $C_{10}H_{16}O_7$ as the lead HOM compound. In the two experiments with seed present (_Exp2.1_ and _Exp3_) we had SOA yields of 7.3 % and 10.0 % at high HO_2/RO_2 and 10.0 % and 12.8 % at low HO_2/RO_2. The difference in the SOA yields between experiments can be explained by the slightly different OH concentrations and subsequent difference in contribution by photooxidation (see **Table 1**). Overall, our yields are in the lower range in comparison with the SOA yields reported by McFiggans et al. (2019) for the α-pinene photooxidation. However, our experiments were also performed at 5 °C higher temperature (20 °C compared to 15 °C in McFiggans et al. (2019)). The SOA yields show an absolute reduction of ~3 % at high HO_2/RO_2 compared to low HO_2/RO_2 (relative a reduction of about 30 %). A reduction of the SOA yield of α-pinene by addition of CO was described before by McFiggans et al. (2019), however, there the α-pinene OH turnover was not held constant.

The change from low to high HO_2/RO_2 regime favored termination reactions to protic termination groups, as we observed less carbonyl compounds and more hydroperoxides. This could overall shift the product distribution to products with lower vapor pressures and favor SOA formation, since protic groups can act as hydrogen bond donors as well as hydrogen bond acceptors. (as exemplified by the comparison of ethanol (boiling point (b.p) 78 °C) and ethane hydroperoxide (b.p. 93-97 °C) with acetaldehyde (b.p. 20 °C) (Richter et al., 1955)). However, the effect of the termination group should be small for HOM as they likely contain multiple hydroperoxide groups (compare Pullinen et al. (2020)). The reduction in HOM-Acc is

638 expected to decrease the condensable mass, since the HOM-Acc scavenge non-HOM-RO_2, that would otherwise not partition

639 into the particle phase.

640 Which of the measured compounds contribute significantly to the organic particle mass can be inferred by comparing their

641 signal from the pure gas phase, unseeded cases to their signal with seed in the system. Under the assumptions that, for most

642 HOM-compounds re-evaporation to the gas phase is negligible and that the precursor chemistry is not substantially disturbed

643 by seed addition, the fraction of signal remaining with seed in the system reflects to which degree the compound is

644 condensing. **Figure 13** shows the fraction remaining with seed in the system plotted against the molar mass of each

645 individual compound. The plot includes all closed shell products that were measured with a relative standard deviation of

646 less than 30 % for all measurement phases and depicts the results for both the high and low HO_2/RO_2 case.
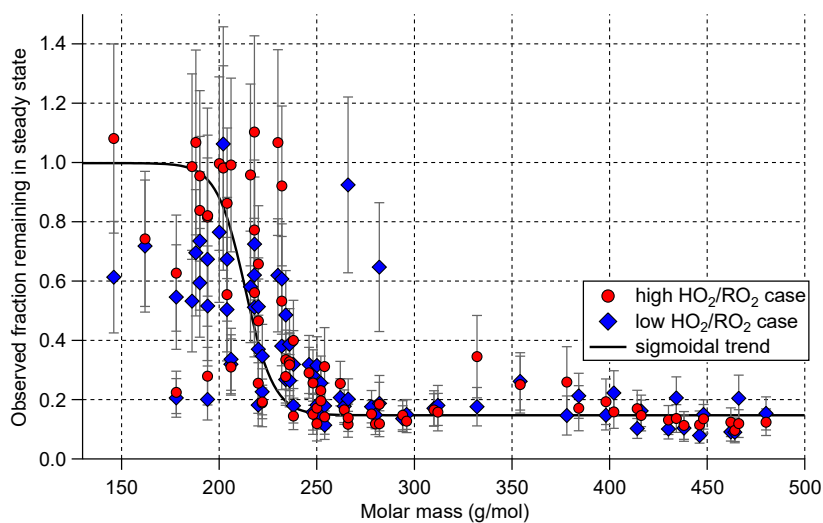
647

648 **Figure 13: Gas-phase fraction remaining in presence of seed (normalization of all data with α-pinene OH turnover) for the low**
649 **(blue) and high (red) HO_2/RO_2 case. Displayed points represent all closed-shell compounds that were detected with relative**
650 **standard deviation <30 % in all four experiment phases. Error bars represent result of error propagation (see supplement**
651 **Sect. S9)**

652 Overall, in both cases we observed the same trend. Lighter compounds are not affected by the presence of seed particles, but

653 with increasing molar mass the fraction remaining in the gas phase is reduced. A difference between the low and high

654 HO_2/RO_2 case can be observed in the low molar mass range: In the high HO_2/RO_2 case many fragmentation products show a

655 higher gas-phase fraction remaining up to 1. (In some cases, values larger than 1 were observed, however within the error

656 limits. For the error estimation see supplement **Sect. S9**). Fractions remaining larger than 1 beyond error could be an

657 indication that such products have a particle-phase production source. **Figure 13** also shows a critical SVOC/LVOC region

658 for molar masses between 175 g mol^{-1} and 250 g mol^{-1} where neither a fraction remaining of 1 nor complete condensation is

659 observed. The position of this region on the molar mass scale depends on the provided organic mass concentration. The large

660 variation of the fraction remaining in this small range of molar masses shows that the partitioning coefficients are dependent

661   on the detailed structure of the compounds and not simply on their molar mass. The semi-volatile and low volatility products

662   represent mainly higher oxidized fragments and HOM-Mon with less than 8 oxygen.

663   For compounds with a molar mass larger than 250 g mol^{-1} a constant fraction remaining is reached in steady state, which is

664   due to an ongoing production of the compounds. From the condensation behavior shown in **Fig. 13** we conclude that the

665   compounds heavier than 230 g mol^{-1} are expected to be of sufficiently low volatility to be mainly found in the particle phase

666   for the organic mass present in the system and therefore contribute significantly to the SOA mass formation. Our finding

667   agrees with the threshold used for low volatility HOM products in Pullinen et al. (2020).

668   Therefore, the signal of all compounds with a molar mass heavier than 230 g mol^{-1} was weighted with their molar mass and

669   summed (see **Eq. (2)**). The ratio of this weighted signal sum at low and high HO$_2$/RO$_2$ is then a measure of expected SOA

670   mass loss. The calculation leads to an expected reduction to 72 % (blue bar, **Fig. 14**). This simplified approach leads to a

671   good agreement with the AMS measurements and can thus explain the reduced particulate organic mass within the errors.
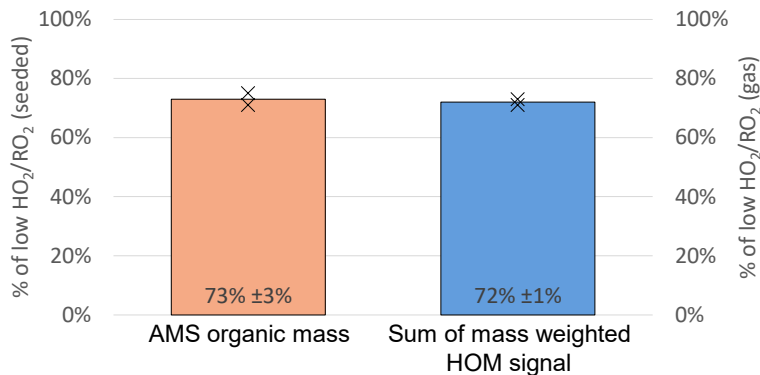
672

673   **Figure 14: Overview of the average, relative change in organic mass observed in the AMS (left y-axis, seeded experiments) and the**
674   **mass weighted HOM signal observed in the NO$_3$-CIMS (right y-axis, unseeded experiments) between the low and high HO$_2$/RO$_2$**
675   **case (both normalized to α-pinene OH turnover).**

676   To test for closure between HOM lost and particulate organic mass measured we approximated the upper limit of HOM

677   concentration in the condensed phase. For this calculation we used the calibration factor determined for sulfuric acid for our

678   NO$_3$-MION-CIMS (7.0·10^9 molecules· cm^{-3}·ncps^{-1}) and the relationship between gas and particulate concentration of a

679   compound in the SAPHIR STAR chamber described in **Eq. (3)**. Again, we considered all compounds with M>230 g mol^{-1} in

680   our calculation. The summed mass concentration lost from the gas phase was then compared to the SOA mass measured in

681   the AMS. This comparison yields a good agreement within the uncertainties. The detailed calculation results can be found in

682   the supplement (**Fig. S3**). Overall, an agreement within 40 % is achieved for all measurement stages.

683 The comparisons presented above show that we understand the processes governing the SOA formation in our chamber and
684 that the NO_3-CIMS measurements are well suited to observe the critical changes to understand the reduction in condensable
685 organic material when shifting from low to high HO_2/RO_2.

5   Conclusion

687 In the presented series of experiments, we achieved a shift from a RO_2+RO_2 dominated chemistry to a more atmospherically
688 relevant HO_2/RO_2 ratio under constant α-pinene OH turnover. It was shown that moving towards atmospheric HO_2/RO_2 ratio
689 affected the SOA formation potential, with the observed organic mass being reduced at high HO_2/RO_2. This is in support of
690 the potential bias towards high SOA yields in chamber studies at low HO_2/RO_2 as discussed by Schervish and Donahue
691 (2021). Our results confirm that too low HO_2/RO_2 is one important parameter that can lead to an overestimated SOA yield in
692 laboratory studies. In a broader picture the results show how important it is to consider the different contributions to the
693 HOM-RO_2 sink (e.g. HO_2, RO_2. NO) when designing experiments and transferring laboratory results to the real atmosphere.

694 The gas-phase observations showed that the SOA reduction at high HO_2/RO_2 was mainly due to a reduced HOM-Acc
695 formation which were formed by RO_2+RO_2 cross reactions in the low HO_2/RO_2 cases. This prevented contribution to SOA
696 by less oxidized RO_2 which were scavenged in the HOM-Acc at low HO_2/RO_2. Under atmospheric condition such cross
697 reactions are less important, and such (mixed) accretion products would contribute less to SOA.

698 The overall observed HOM-products were reduced slightly, showing that under certain circumstances RO_2+HO_2 termination
699 can impede the HOM formation, mainly by reducing the precursor RO_2 levels and less by impeding the autoxidation itself.
700 The autoxidation chain (once initiated) runs to a similar oxidation level at both high and low HO_2/RO_2. The observed
701 HOM-Mon products shift significantly between monomer families due to the different termination reaction. A decrease in
702 carbonyl and alcohol formation from RO_2+RO_2 and an increase in hydroperoxide formation from RO_2+HO_2 was observed at
703 high HO_2/RO_2.

704 Furthermore, a reduction in HOM-Frag products, especially with lower carbon numbers, as well as the parity of the $C_{10}H_{15}O_x$
705 HOM-RO_2 show a reduction in alkoxy radical formation at high HO_2/RO_2. The moderate reduction in larger HOM-Frag
706 products and pinonaldehyde, however, suggest that some alkoxy radical steps are still important. This raises the question of
707 whether alkoxy radical formation can be facilitated by HO_2. In the atmosphere such effects are most often overcome
708 whenever RO_2+NO is the major alkoxy radical source.

709 Overall, the observed changes in the gas phase could be well explained with the presented generic mechanistic understanding
710 of HOM formation in the α-pinene system. The addition of seed demonstrated that the shift towards high HO_2/RO_2 reduced
711 the condensable organic mass, stressing the importance of controlling higher order reactions of peroxy radicals which lead to
712 overemphasis of HOM-Acc product formation at low HO_2/RO_2 ratios.

713 Furthermore, the seed addition allowed us to determine which products were contributing to the SOA formation and show

714 that their volatility is a function of molar mass and detailed molecular structure. This revealed a critical mass region in which

715 compounds have significant fractions in gas and particulate phase. Based on absorptive partitioning theory the volatilities at

716 which this critical region is found should depend on the organic mass present in the system.

717 Valuable insight about the condensed phase can be gained from HOM gas phase measurements. We inferred conclusions

718 about the particulate phase from the gas phase measurements and compared them to the direct particle phase observations,

719 finding good agreements between our expectations and the measurements.

Data availability
721 All presented data will be available in a repository before the submission of the final manuscript.

Author contribution
723 TFM, MH and GM conceptualized the study and TFM, YB, SK and SRZ designed the experiments and developed the

724 analysis methodology. The experiments were performed by YB, SK, VG and SRZ. Instrument deployment and/or data

725 analysis were performed by YB, SK, HW, RW, JX, AZ, QH, TZ and VG. YB did model calculations of the experiments.

726 AV, SPO, TJB, MG and MH provided counsel on experiment design and data interpretation. The compiled data set was

727 interpreted by YB and TFM, and the results were discussed by all co-authors. YB visualized the data and YB and TFM

728 prepared the manuscript. All co-authors reviewed the manuscript.

Competing interests
730 The authors declare that they have no conflict of interest.

Financial support
732 This research has received funding from the European Union's Horizon 2020 research and innovation programme under the

733 FORCeS grant agreement No 821205, the Federal Ministry of Education and Research (BMBF) Germany under the FONA

734 Strategy "Research for Sustainability" as part of the implementation of ACTRIS-D under the funding code 01LK200010,

735 Vetenskapsrådet (VR, grant agreement No. 2018-04430), Svenska Forskningsrådet Formas (grant agreement No. 2019-586)

736 and the Natural Environment Research Council (NERC) UK under the grant agreement No. NE/V012665/1.

References

Albrecht, S. R., Novelli, A., Hofzumahaus, A., Kang, S., Baker, Y., Mentel, T., Wahner, A., and Fuchs, H.: Measurements of hydroperoxy radicals (HO2) at atmospheric concentrations using bromide chemical ionisation mass spectrometry, Atmos. Meas. Tech., 12, 891-902, https://doi.org/10.5194/amt-12-891-2019, 2019.

Atkinson, R. and Arey, J.: Atmospheric degradation of volatile organic compounds, Chem. Rev., 103, 4605-4638, https://doi.org/10.1021/cr0206420, 2003.

Berndt, T.: Peroxy Radical Processes and Product Formation in the OH Radical-Initiated Oxidation of α-Pinene for Near-Atmospheric Conditions, J. Phys. Chem. A, 125, 9151-9160, https://doi.org/10.1021/acs.jpca.1c05576, 2021.

Berndt, T., Mentler, B., Scholz, W., Fischer, L., Herrmann, H., Kulmala, M., and Hansel, A.: Accretion product formation from ozonolysis and OH radical reaction of α-pinene: mechanistic insight and the influence of isoprene and ethylene, Environ. Sci. Technol., 52, 11069-11077, https://doi.org/10.1021/acs.est.8b02210, 2018.

Berndt, T., Richters, S., Jokinen, T., Hyttinen, N., Kurtén, T., Otkjaer, R. V., Kjaergaard, H. G., Stratmann, F., Herrmann, H., Sipila, M., Kulmala, M., and Ehn, M.: Hydroxyl radical-induced formation of highly oxidized organic compounds, Nat. Commun., 7, 13677, https://doi.org/10.1038/ncomms13677, 2016.

Bianchi, F., Garmash, O., He, X. C., Yan, C., Iyer, S., Rosendahl, I., Xu, Z. N., Rissanen, M. P., Riva, M., Taipale, R., Sarnela, N., Petäjä, T., Worsnop, D. R., Kulmala, M., Ehn, M., and Junninen, H.: The role of highly oxygenated molecules (HOMs) in determining the composition of ambient ions in the boreal forest, Atmos. Chem. Phys., 17, 13819-13831, https://doi.org/10.5194/acp-17-13819-2017, 2017.

Bianchi, F., Kurtén, T., Riva, M., Mohr, C., Rissanen, M. P., Roldin, P., Berndt, T., Crounse, J. D., Wennberg, P. O., Mentel, T. F., Wildt, J., Junninen, H., Jokinen, T., Kulmala, M., Worsnop, D. R., Thornton, J. A., Donahue, N., Kjaergaard, H. G., and Ehn, M.: Highly Oxygenated Organic Molecules (HOM) from Gas-Phase Autoxidation Involving Peroxy Radicals: A Key Contributor to Atmospheric Aerosol, Chem. Rev., 119, 3472-3509, https://doi.org/10.1021/acs.chemrev.8b00395, 2019.

Cox, R. A., Ammann, M., Crowley, J. N., Herrmann, H., Jenkin, M. E., McNeill, V. F., Mellouki, A., Troe, J., and Wallington, T. J.: Evaluated kinetic and photochemical data for atmospheric chemistry: Volume VII – Criegee intermediates, Atmos. Chem. Phys., 20, 13497-13519, https://doi.org/10.5194/acp-20-13497-2020, 2020.

Crounse, J. D., Nielsen, L. B., Jørgensen, S., Kjaergaard, H. G., and Wennberg, P. O.: Autoxidation of organic compounds in the atmosphere, J. Phys. Chem. Lett., 4, 3513-3520, https://doi.org/10.1021/jz4019207, 2013.

Docherty, K. S. and Ziemann, P. J.: Effects of stabilized criegee intermediate and OH radical scavengers on aerosol formation from reactions of β-pinene with O3, Aerosol Sci. Tech., 37, 877-891, https://doi.org/10.1080/02786820300930, 2003.

Eddingsaas, N., Loza, C., Yee, L., Seinfeld, J., and Wennberg, P.: α-Pinene photooxidation under controlled chemical conditions – Part 1: Gas-phase composition in low- and high-NOx environments, Atmos. Chem. Phys., 12, 6489-6504, https://doi.org/10.5194/acp-12-6489-2012, 2012.

Ehn, M., Thornton, J. A., Kleist, E., Sipila, M., Junninen, H., Pullinen, I., Springer, M., Rubach, F., Tillmann, R., Lee, B., Lopez-Hilfiker, F., Andres, S., Acir, I. H., Rissanen, M., Jokinen, T., Schobesberger, S., Kangasluoma, J., Kontkanen, J., Nieminen, T., Kurtén, T., Nielsen, L. B., Jorgensen, S., Kjaergaard, H. G., Canagaratna, M., Maso, M. D., Berndt, T., Petaja, T., Wahner, A., Kerminen, V. M., Kulmala, M., Worsnop, D. R., Wildt, J., and Mentel, T. F.: A large source of low-volatility secondary organic aerosol, Nature, 506, 476-479, https://doi.org/10.1038/nature13032, 2014.

Eisele, F. and Tanner, D.: Measurement of the gas phase concentration of H2SO4 and methane sulfonic acid and estimates of H2SO4 production and loss in the atmosphere, J. Geophys. Res. Atmos., 98, 9001-9010, https://doi.org/10.1029/93JD00031, 1993.

Fantechi, G., Vereecken, L., and Peeters, J.: The OH-initiated atmospheric oxidation of pinonaldehyde: Detailed theoretical study and mechanism construction, Phys. Chem. Chem. Phys., 4, 5795-5805, https://doi.org/10.1039/B205901K 2002.

Guo, Y., Shen, H., Pullinen, I., Luo, H., Kang, S., Vereecken, L., Fuchs, H., Hallquist, M., Acir, I. H., Tillmann, R., Rohrer, F., Wildt, J., Kiendler-Scharr, A., Wahner, A., Zhao, D. F., and Mentel, T. F.: Identification of highly oxygenated organic molecules and their role in aerosol formation in the reaction of limonene with nitrate radical, Atmos. Chem. Phys., 22, 11323-11346, https://doi.org/10.5194/acp-22-11323-2022, 2022.

Hallquist, M., Wenger, J. C., Baltensperger, U., Rudich, Y., Simpson, D., Claeys, M., Dommen, J., Donahue, N. M., George, C., Goldstein, A. H., Hamilton, J. F., Herrmann, H., Hoffmann, T., Iinuma, Y., Jang, M., Jenkin, M. E., Jimenez, J. L., Kiendler-Scharr, A., Maenhaut, W., McFiggans, G., Mentel, T. F., Monod, A., Prévôt, A. S. H., Seinfeld, J. H., Surratt, J. D., Szmigielski, R., and Wildt, J.: The formation, properties and impact of secondary organic aerosol: current and emerging issues, Atmos. Chem. Phys., 9, 5155-5236, https://doi.org/10.5194/acp-9-5155-2009, 2009.

Hantschke, L. L.: Oxidation of monoterpenes studied in atmospheric simulation chambers, Forschungszentrum Jülich GmbH, Zentralbibliothek, Verlag, 2022.

Hasson, A. S., Kuwata, K. T., Arroyo, M. C., and Petersen, E. B.: Theoretical studies of the reaction of hydroperoxy radicals (HO2) with ethyl peroxy (CH3CH2O2), acetyl peroxy (CH3C(O)O2), and acetonyl peroxy (CH3C(O)CH2O2) radicals, J. Photochem. Photobiol. A, 176, 218-230, https://doi.org/10.1016/j.jphotochem.2005.08.012, 2005.

Henry, K. M., Lohaus, T., and Donahue, N. M.: Organic aerosol yields from α-pinene oxidation: bridging the gap between first-generation yields and aging chemistry, Environ. Sci. Technol., 46, 12347-12354, https://doi.org/10.1021/es302060y, 2012.

Hidy, G.: Atmospheric chemistry in a box or a bag, Atmos., 10, 401, https://doi.org/10.3390/atmos10070401, 2019.

Hyttinen, N., Otkjær, R. V., Iyer, S., Kjaergaard, H. G., Rissanen, M. P., Wennberg, P. O., and Kurtén, T.: Computational comparison of different reagent ions in the chemical ionization of oxidized multifunctional compounds, J. Phys. Chem. A, 122, 269-279, https://doi.org/10.1021/acs.jpca.7b10015, 2018.

Iyer, S., Reiman, H., Møller, K. H., Rissanen, M. P., Kjaergaard, H. G., and Kurtén, T.: Computational investigation of RO2+ HO2 and RO2+ RO2 reactions of monoterpene derived first-generation peroxy radicals leading to radical recycling, J. Phys. Chem. A, 122, 9542-9552, https://doi.org/10.1021/acs.jpca.8b09241, 2018.

Iyer, S., Rissanen, M. P., Valiev, R., Barua, S., Krechmer, J. E., Thornton, J., Ehn, M., and Kurtén, T.: Molecular mechanism for rapid autoxidation in α-pinene ozonolysis, Nat. Commun., 12, 878, https://doi.org/10.1038/s41467-021-21172-w, 2021.

Jenkin, M. E., Saunders, S. M., and Pilling, M. J.: The tropospheric degradation of volatile organic compounds: a protocol for mechanism development, Atmos. Environ., 31, 81-104, https://doi.org/10.1016/S1352-2310(96)00105-7, 1997.

Jenkin, M. E., Valorso, R., Aumont, B., and Rickard, A. R.: Estimation of rate coefficients and branching ratios for reactions of organic peroxy radicals for use in automated mechanism construction, Atmos. Chem. Phys., 19, 7691-7717, https://doi.org/10.5194/acp-19-7691-2019, 2019.

Johnson, D. and Marston, G.: The gas-phase ozonolysis of unsaturated volatile organic compounds in the troposphere, Chem. Soc. Rev., 37, 699-716, https://doi.org/10.1039/B704260B 2008.

Junninen, H., Ehn, M., Petäjä, T., Luosujärvi, L., Kotiaho, T., Kostiainen, R., Rohner, U., Gonin, M., Fuhrer, K., Kulmala, M., and Worsnop, D. R.: A high-resolution mass spectrometer to measure atmospheric ion composition, Atmos. Meas. Tech., 3, 1039-1053, https://doi.org/10.5194/amt-3-1039-2010, 2010.

Kang, S.: Formation of highly oxygenated organic molecules from α-pinene photochemistry, Forschungszentrum Jülich GmbH, 2021.

Keywood, M., Kroll, J., Varutbangkul, V., Bahreini, R., Flagan, R., and Seinfeld, J.: Secondary organic aerosol formation from cyclohexene ozonolysis: Effect of OH scavenger and the role of radical chemistry, Environ. Sci. Technol., 38, 3343-3350, https://doi.org/10.1021/es049725j, 2004.

Khan, M., Cooke, M., Utembe, S., Archibald, A., Derwent, R., Jenkin, M. E., Morris, W., South, N., Hansen, J., Francisco, J., Percival, C. J., and Shallcross, D. E.: Global analysis of peroxy radicals and peroxy radical-water complexation using the STOCHEM-CRI global chemistry and transport model, Atmospheric Environment, 106, 278-287, https://doi.org/10.1016/j.atmosenv.2015.02.020, 2015.

Kiendler-Scharr, A., Wildt, J., Maso, M. D., Hohaus, T., Kleist, E., Mentel, T. F., Tillmann, R., Uerlings, R., Schurr, U., and Wahner, A.: New particle formation in forests inhibited by isoprene emissions, Nature, 461, 381-384, https://doi.org/10.1038/nature08292, 2009.

McFiggans, G., Mentel, T. F., Wildt, J., Pullinen, I., Kang, S., Kleist, E., Schmitt, S., Springer, M., Tillmann, R., Wu, C., Zhao, D., Hallquist, M., Faxon, C., Le Breton, M., Hallquist, A. M., Simpson, D., Bergstrom, R., Jenkin, M. E., Ehn, M., Thornton, J. A., Alfarra, M. R., Bannan, T. J., Percival, C. J., Priestley, M., Topping, D., and Kiendler-Scharr, A.: Secondary organic aerosol reduced by mixture of atmospheric vapours, Nature, 565, 587-593, https://doi.org/10.1038/s41586-018-0871-y, 2019.

Mentel, T., Springer, M., Ehn, M., Kleist, E., Pullinen, I., Kurtén, T., Rissanen, M., Wahner, A., and Wildt, J.: Formation of highly oxidized multifunctional compounds: autoxidation of peroxy radicals formed in the ozonolysis of alkenes–deduced from structure–product relationships, Atmos. Chem. Phys., 15, 6745-6765, https://doi.org/10.5194/acp-15-6745-2015, 2015.

Mentel, T. F., Wildt, J., Kiendler-Scharr, A., Kleist, E., Tillmann, R., Dal Maso, M., Fisseha, R., Hohaus, T., Spahn, H., Uerlings, R., Wegener, R., Griffiths, P. T., Dinar, E., Rudich, Y., and Wahner, A.: Photochemical production of aerosols from real plant emissions, Atmos. Chem. Phys., 9, 4387-4406, https://doi.org/10.5194/acp-9-4387-2009, 2009.

Mohr, C., Thornton, J. A., Heitto, A., Lopez-Hilfiker, F. D., Lutz, A., Riipinen, I., Hong, J., Donahue, N. M., Hallquist, M., Petaja, T., Kulmala, M., and Yli-Juuti, T.: Molecular identification of organic vapors driving atmospheric nanoparticle growth, Nat. Commun., 10, 4442, https://doi.org/10.1038/s41467-019-12473-2, 2019.

Otkjaer, R. V., Jakobsen, H. H., Tram, C. M., and Kjaergaard, H. G.: Calculated Hydrogen Shift Rate Constants in Substituted Alkyl Peroxy Radicals, J. Phys. Chem. A, 122, 8665-8673, https://doi.org/10.1021/acs.jpca.8b06223, 2018.

Piletic, I. R. and Kleindienst, T. E.: Rates and yields of unimolecular reactions producing highly oxidized peroxy radicals in the OH-induced autoxidation of α-pinene, β-pinene, and limonene, J. Phys. Chem. A, 126, 88-100, https://doi.org/10.1021/acs.jpca.1c07961, 2022.

Pullinen, I., Schmitt, S., Kang, S., Sarrafzadeh, M., Schlag, P., Andres, S., Kleist, E., Mentel, T. F., Rohrer, F., Springer, M., Tillmann, R., Wildt, J., Wu, C., Zhao, D., Wahner, A., and Kiendler-Scharr, A.: Impact of NOx on secondary organic aerosol

849 (SOA) formation from α-pinene and β-pinene photooxidation: the role of highly oxygenated organic nitrates, Atmos. Chem.
850 Phys., 20, 10125-10147, https://doi.org/10.5194/acp-20-10125-2020, 2020.

851 Richter, F., Ostertag, R., Ammerlahn, G., Behrle, E., Baumann, M., and Kobel, M.: Beilstein's handbook of organic
852 chemistry. Third supplement, covering the literature from 1930-1949, 1955.

853 Rissanen, M. P., Mikkilä, J., Iyer, S., and Hakala, J.: Multi-scheme chemical ionization inlet (MION) for fast switching of
854 reagent ion chemistry in atmospheric pressure chemical ionization mass spectrometry (CIMS) applications, Atmos. Meas.
855 Tech., 12, 6635-6646, https://doi.org/10.5194/amt-12-6635-2019, 2019.

856 Rissanen, M. P., Kurtén, T., Sipila, M., Thornton, J. A., Kangasluoma, J., Sarnela, N., Junninen, H., Jorgensen, S.,
857 Schallhart, S., Kajos, M. K., Taipale, R., Springer, M., Mentel, T. F., Ruuskanen, T., Petaja, T., Worsnop, D. R., Kjaergaard,
858 H. G., and Ehn, M.: The formation of highly oxidized multifunctional products in the ozonolysis of cyclohexene, J. Am.
859 Chem. Soc., 136, 15596-15606, https://doi.org/10.1021/ja507146s, 2014.

860 Roldin, P., Ehn, M., Kurtén, T., Olenius, T., Rissanen, M. P., Sarnela, N., Elm, J., Rantala, P., Hao, L., Hyttinen, N.,
861 Heikkinen, L., Worsnop, D. R., Pichelstorfer, L., Xavier, C., Clusius, P., Öström, E., Petäjä, T., Kulmala, M., Vehkamäki,
862 H., Virtanen, A., Riipinen, I., and Boy, M.: The role of highly oxygenated organic molecules in the Boreal aerosol-cloud-
863 climate system, Nat. Commun., 10, 4370, https://doi.org/10.1038/s41467-019-12338-8, 2019.

864 Sanchez, J., Tanner, D. J., Chen, D., Huey, L. G., and Ng, N. L.: A new technique for the direct detection of HO2 radicals
865 using bromide chemical ionization mass spectrometry (Br-CIMS): initial characterization, Atmos. Meas. Tech., 9, 3851-
866 3861, https://doi.org/10.5194/amt-9-3851-2016, 2016.

867 Sarrafzadeh, M., Wildt, J., Pullinen, I., Springer, M., Kleist, E., Tillmann, R., Schmitt, S. H., Wu, C., Mentel, T. F., Zhao,
868 D., Hastie, D. R., and Kiendler-Scharr, A.: Impact of NOx and OH on secondary organic aerosol formation from β-pinene
869 photooxidation, Atmos. Chem. Phys., 16, 11237-11248, https://doi.org/10.5194/acp-16-11237-2016, 2016.

870 Saunders, S. M., Jenkin, M. E., Derwent, R., and Pilling, M.: Protocol for the development of the Master Chemical
871 Mechanism, MCM v3 (Part A): tropospheric degradation of non-aromatic volatile organic compounds, Atmos. Chem. Phys.,
872 3, 161-180, https://doi.org/10.5194/acp-3-161-2003, 2003.

873 Schervish, M. and Donahue, N. M.: Peroxy radical kinetics and new particle formation, Environ. Sci. Atmos., 1, 79-92,
874 https://doi.org/10.1039/d0ea00017e, 2021.

875 Shen, H., Vereecken, L., Kang, S., Pullinen, I., Fuchs, H., Zhao, D., and Mentel, T. F.: Unexpected significance of a minor
876 reaction pathway in daytime formation of biogenic highly oxygenated organic compounds, Sci. Adv., 8, eabp8702,
877 https://doi.org/10.1126/sciadv.abp8702, 2022.

878 Shen, H., Zhao, D., Pullinen, I., Kang, S., Vereecken, L., Fuchs, H., Acir, I. H., Tillmann, R., Rohrer, F., Wildt, J., Kiendler-
879 Scharr, A., Wahner, A., and Mentel, T. F.: Highly Oxygenated Organic Nitrates Formed from NO(3) Radical-Initiated
880 Oxidation of β-Pinene, Environ. Sci. Technol., 55, 15658-15671, https://doi.org/10.1021/acs.est.1c03978, 2021.

881 Shilling, J. E., Chen, Q., King, S. M., Rosenoern, T., Kroll, J. H., Worsnop, D. R., DeCarlo, P. F., Aiken, A. C., Sueper, D.,
882 Jimenez, J. L., and Martin, S. T.: Loading-dependent elemental composition of α-pinene SOA particles, Atmos. Chem.
883 Phys., 9, 771-782, https://doi.org/10.5194/acp-9-771-2009, 2009.

884 Vereecken, L. and Nozière, B.: H migration in peroxy radicals under atmospheric conditions, Atmos. Chem. Phys., 20, 7429-
885 7458, https://doi.org/10.5194/acp-20-7429-2020, 2020.

886 Vereecken, L., Müller, J.-F., and Peeters, J.: Low-volatility poly-oxygenates in the OH-initiated atmospheric oxidation of α-
887 pinene: impact of non-traditional peroxyl radical chemistry, Phys. Chem. Chem. Phys., 9, 5241-5248,
888 https://doi.org/10.1039/b708023a, 2007.

889 Wildt, J., Mentel, T. F., Kiendler-Scharr, A., Hoffmann, T., Andres, S., Ehn, M., Kleist, E., Müsgen, P., Rohrer, F., Rudich,
890 Y., Springer, M., Tillmann, R., and Wahner, A.: Suppression of new particle formation from monoterpene oxidation by
891 NOx, Atmos. Chem. Phys., 14, 2789-2804, https://doi.org/10.5194/acp-14-2789-2014, 2014.

892 Xu, L., Møller, K. H., Crounse, J. D., Otkjær, R. V., Kjaergaard, H. G., and Wennberg, P. O.: Unimolecular reactions of
893 peroxy radicals formed in the oxidation of α-pinene and β-pinene by hydroxyl radicals, J. Phys. Chem. A, 123, 1661-1674,
894 https://doi.org/10.1021/acs.jpca.8b11726, 2019.
895